Thermo-mechanical Stress Analysis of Functionally Graded Tapered Shaft System

A THESIS SUBMITTED IN THE PARTIAL FULFILLMENT OF THE REQUIREMENTS FOR THE DEGREE OF

Master of Technology

In

MECHANICAL ENGINEERING

[Specialization: Machine Design and Analysis]

By

Dinesh Patil

(213ME1385)

DEPARTMENT OF MECHANICAL ENGINEERING

NATIONAL INSTITUTE OF TECHNOLOGY

ROURKELA – 769008

JUNE, 2015

Thermo-mechanical Stress Analysis of Functionally Graded Tapered Shaft System

A THESIS SUBMITTED IN THE PARTIAL FULFILLMENT OF THE REQUIREMENTS FOR THE DEGREE OF

Master of Technology

In

MECHANICAL ENGINEERING

[Specialization: Machine Design and Analysis]

By

Dinesh Patil

(213ME1385)

Under the Supervision of

Prof. Tarapada Roy

DEPARTMENT OF MECHANICAL ENGINEERING

NATIONAL INSTITUTE OF TECHNOLOGY

ROURKELA – 769008

JUNE, 2015

National Institute of Technology
Rourkela

CERTIFICATE

This is to certify that the thesis entitled, ***"Thermo-mechanical Stress Analysis of Functionally Graded Tapered Shaft System"*** *submitted by* ***Mr. Dinesh Patil,*** *Roll No.* ***213ME1385*** *in partial fulfilment of the requirements for the award of* ***Master of Technology*** *Degree in* ***Mechanical Engineering*** *with specialization in* ***"Machine Design and Analysis"*** *at National Institute of Technology, Rourkela is an authentic work carried out by him under my supervision and guidance. To the best of my knowledge, the matter embodied in this thesis has not been submitted to any other university/ institute for award of any Degree or Diploma.*

Date: 01 June 2015

Prof. Tarapada Roy
Dept. of Mechanical Engineering
National Institute of Technology,
Rourkela -769008

DEPARTMENT OF MECHANICAL ENGINEERING

NATIONAL INSTITUTE OF TECHNOLOGY

ROURKELA 769008

ACKNOWLEDGEMENT

It gives me immense pleasure to express my deep sense of gratitude to my supervisor **Prof. Tarapada Roy** for his invaluable guidance, motivation, constant inspiration and above all for his ever co-operating attitude that enabled me to bring up this thesis to the present form.

I express my sincere thanks to the Director, **Prof. S.K.Sarangi,** National Institute of Technology, Rourkela for motivating me in this endeavour and providing me the necessary facilities for this study.

I would like to extend my thanks to Ph.D. scholars, **D Koteswara Rao** and **Ashirbad Swain**, Department of Mechanical Engineering, NIT Rourkela for their support and guidance during my project work.

Last but not the least; I would like to express my love, respect and gratitude to **my parents** and **my brother-in-law**, who have always supported me in every decision I have made, guided me in every turn of my life, believed in me and my potential and without whom I would have never been able to achieve whatsoever I could have till date.

Place: Rourkela

Date**:** 01 June 2015

Dinesh Patil

M. Tech., Roll No: 213ME1385

Machine Design and Analysis

Department of Mechanical Engineering

National Institute of Technology, Rourkela

CONTENTS

List of Figures

List of Tables

ABSTRACT

Present work deals with the study of stresses developed in tapered functionally graded (FG) shaft system under both thermal and mechanical environment for three nodded beam element by using Timoshenko beam theory. The temperature distribution in radial direction is assumed based on one dimensional steady state temperature field by Fourier heat conduction equation without considering heat generation. Temperature dependent material properties are varied along the radial direction using power law gradation. Tapered FG shaft consists of rigid disk attached at its centre and shaft is mounted on two flexible bearings acts as spring and damper, inner radius of the tapered shaft is varying in x direction keeping thickness of hollow tapered shaft is constant. For the present analysis the Mixture of Stainless steel (SUS304) and Aluminum oxide (Al_2O_3) are considered as inner and outer surface material of the FG shaft. Three dimensional constitutive relations are derived based on first order shear deformation theory (FSDT) for Timoshenko beam element considering rotary inertia, strain and kinetic energy of shaft and gyroscopic effect. In present study, structural and hysteretic damping are incorporated. Hamilton's principle is used to derive governing equation of motion for three nodded beam element for six degree of freedom per node. Complete MATLB code is generated and shows that temperature field and power law gradient index have important part on material properties. Comparative study is carried out for Stainless steel and FG tapered shaft, shows that stress developed in FG shaft is comparatively lower than Steel shaft. Various results are obtained for coupled and uncoupled environment. Transient stress are obtained for varying power law index value and speed as a parameter. Stress amplitude increases for increase in speed and power law index. Results achieved for FG shaft shows advantages over steel shaft.

Keywords: Functionally graded materials (FGMs), Power law index, Tapered shaft, Timoshenko beam theory (TBT), Three nodded beam element, Finite element method, Thermo-mechanical, Stress analysis.

CHAPTER 1

INTRODUCTION

Composite materials are materials, composed of two or more fundamental materials with different properties, when combined to get a material with different properties than that of individual constituents. Composite material structures are more frequently used in engineering fields as their high strength to weight ratio and high stiffness to weight ratio is basically favourable for material selection. Main disadvantage with composite material is, weakness in interface between neighbouring layers, which is popularly known as delamination phenomenon that may cause structural failure. To overcome this problem, a new class of material presented, named as Functionally Graded Materials (FGMs). FGMs are recognised as, whose material properties are varying in certain direction and thus overcome interface weakness. FGMs are defined as, the materials whose volume fractions of two or more materials are varied continuously along certain direction to attain required purpose. FGMs provide better material response and excellent performance in thermal environments like thermal barrier and space application, where it is used to protect space shuttle from heat generated during re-entry to Earth's atmosphere by modelling ceramic material at outer surface metal at inside surface.

Because of high strength, stiffness and low density material characteristics, brings an idea for replacing conventional metallic shafts with FGMs rotor shaft in many application areas like design of spinning components such as driveshaft in automobiles, jet engines and helicopters, turbine shafts and other rotating machineries. Composite materials has been validated both numerically and experimentally in rotor dynamics applications. Along with this various new advanced composite materials and material models for rotor shaft has been developed by researchers.

1.1 Background of Rotor Dynamics

Rotor dynamics has a significant history, mainly due to its relationship with theory and practice. Rotor dynamics is a particular branch of applied mechanics deals with the performance and analysis of rotor assemblies. Rotor dynamics mostly used to analyse the performance of a

turbine shafts, jet engine to auto engines and computer storage disks. Basically Rotor dynamics deals with rotor and stator. Rotating part in mechanical devices are called rotors, which are supported on bearings, thus shaft rotate freely about its axis. Many engineering components are deals with the subject of Rotor dynamics and which gives better solution for components like turbines, compressors, alternators, blowers, motors, pumps, brakes etc.

Rotor delivers with behaviour of materials to limit their spin axis in a more or rigid way to a fixed position in space, those are mentioned to as fixed rotor (considering spin speed is constant), while rotors which are not considering in any way are mentioned as free rotors (considering spin speed is governed by conservation of angular momentum). In process, Rotors have excessive deal with rotational energy and small amount of vibrational energy.

In the field of Rotor Dynamics William John Macquorn Rankine (1869) implemented the first analysis of rotating shaft. Considering two degree of freedom shaft model attached with rigid mass whirling in an orbit, having elastic spring acting in radial direction. Whirling speed of the shaft has defined, shows that radial deflection of Rankin's model increases beyond this whirling speed, this speed is termed as threshold speed for the divergent instability.

Swedish engineer Carl Gustaf Patrik de Laval (1833), for marine application he established a single-stage steam impulse turbine and achieved 42000 RPM. He used initially a rigid rotor and then used flexible rotor to operate above critical speed by running at a speed around seven times the critical speed.

Stanley Dunkerley (1895) studied the pulley loaded vibration of shafts. It is known that shafts are well balanced when rotating at particular speed, bends except the amount of deflection is restricted, even shafts may break, though shafts runs at high speed. This critical speed is depends on the way in which shaft is supported, modulus of elasticity, size, weight of the shaft and position of mass (pulleys). German civil engineer August Foppl (1895) presented another rotor model showing stable response above whirling speed. W. kerr (1916) showed experimentally that, second critical aped will occurred when rotor crosses first critical speed safely. Ludwig Prandtl (1918) studied non-circular cross section Jeffcott rotor.

Henry Jeffcott (1919) modelled and studied behaviour of simple spinning rotor under flexural and dynamic behaviour. Actually in Jeffcott model disk do not wobble. As a result, the

angular velocity vector and angular momentum vector are collinear thus no gyroscopic moments are generates.

Aurel B. Stodola (1924) developed dynamics of elastic continuous rotor having discs without considering gyroscopic moment, balancing of shaft, secondary resonance phenomenon due to gravity effect and methods to determine critical speeds of shafts for variable cross sections, also by using Coriolis accelerations supercritical solutions can be stabilized.

Baker (1933) found and defined that because of contact between rotor and stator system exhibits self-exited vibrations. David M. Smith (1933) found formulas for predicting threshold spin speed for supercritical instability varied through bearing stiffness and also with ratio between external to internal viscous damping. Many variations came closer to practical needs of the rotor dynamic field for Jeffcott rotor model. Prohl's and Myklestad's (1945) analysed instabilities and modelling methods in rotors dynamics by Transfer Matrix Method (TMM).

In 1960s, for exact solution capabilities, numerical methods are established for structural dynamic analysis, rotor dynamics codes and digital computer codes were constructed on TMM method. In 1970s alternative fundamental procedure developed that is Finite Element Method (FEM), developed for solution of beam type of models. In 21st century, rotor dynamics are combined FEM and solids modelling methods to create simulations that adapt the coupled behaviour of disks, elastic shafts and elastic support assemblies into a single, multidimensional-model.

1.2 Composite Materials

Composite materials are materials made by combining two or more materials, in a micro scale form and their elements do not dissolve or fuse into each other, to achieve greater improved properties. These materials are broadly used in many applications like aerospace vehicles, nuclear reactors, buildings, automobile vehicles, turbine parts, medical instruments, sports components and in many civil applications. Laminated composite materials contains of several layers of different fibre reinforced materials, bonded together to get the required properties like strength, stiffness, coefficient of thermal expansion, damping and wear resistance. By changing lamina thickness, material properties and stacking sequence preferred properties of the material can be achieved. As composite materials gives high stiffness to weight ration and high strength to weight

ratio, which motives to use in weight sensitive structures. These kind of structures carry improvement of their structural functions especially in aircraft and space applications.

1.3 Drawbacks of Composite Materials

Even though composite materials gives many advantages over other conventional materials, their main disadvantage are impact load, repeated stress cycles and many more, these causes the separation of layers and weakness at interfaces between neighbouring layers, this type of failure mechanism is known as delamination phenomenon, which may seriously cause failure of structures. Other problems of composite materials are, variation in coefficient of thermal expansion and coefficient of moisture of expansion within the materials will leads to residual stress. These residual stress may cause failure of structures. Stress concentrations near material, geometric interface, which will cause the damage in the form of delamination, matrix cracking and parting of adhesive bond, for anisotropic constitution of laminated composite materials. These difficulties can overcome by avoiding rapid changes in material properties.

1.4 Theoretical Understanding about FGMs

Concept of FGM came for the First time while space plane project was going on in year 1984 in Japan. Materials of kind, would serve the purpose of withstanding a surface temperature of around 2000 K with temperature gradient of 1000 K through a 10mm thickness. Nowadays FGMs are becoming a more popular in Germany. FGMs are those of composite materials where the microstructures or composition of materials are locally different so that a definite variation of indigenous material properties are attained, variation properties are along certain directions. By using gradation factor in FGMs, it can be eliminate the sudden change of material properties as in conventional materials, this gradation will helps to eliminate delamination phenomenon, inter laminar stresses and gives better bonding within material as a whole.

Many components like thin shells, plates, turbine blades and many more machine parts are subjected thermal or combined effect of thermo mechanical loading are more likely to fail by large deflections, buckling and excessive stresses. Thus, in such a condition, FGMs can be used where high temperature environment or high temperature gradient. FGMs are largely manufactured from isotropic constituents such as ceramics and metals. Here ceramic portion acts as thermal barrier

and metallic portion serves as structural support. In this condition ceramic portion delivers heat resistance and corrosion resistance, metallic portion gives strength and toughness.

Many problems arises for traditional materials and composite materials can be significantly solved by using FGMs, as gradual variation of material properties in FGMs gives better stability. This new class of materials and their gradual changes in properties are used to design many components and applicable to many areas.

1.5 Practical Applications of FGMs

As technology and innovations are growing rapidly, it is desired to meet materials and their applications as required. FGMs are new class of materials, which are partially fulfil the present need and requirement in engineering field. FGMs are mainly used in high temperature environment, as properties are required to vary inside the materials. Following are some of noticeable applications for FGMs,

i. Aerospace application (space components, planes, insulations for body, structures, Rocket engine. Aerospace skins, nuclear reactors, vibration control etc.).
ii. Engineering applications (rotor shaft system, cutting tools, turbine blades, valves etc.).
iii. Electronic applications (semiconductors, sensors, substrates etc.).
iv. Chemical industries (Rector Vessels, Heat Exchangers, Heat Pipe etc.).
v. Goods materials (Sports, building materials etc.).
vi. Energy exchangers (Thermo ionic converters, solar cells, thermoelectric generators, Fuel cells etc.).

CHAPTER 2

LITERATURE REVIEW

2.1 Introduction

Great number of research has been done in the field of modelling and analysis of FGM's. Some of important workout has been done and presented in following section. Composite materials possess high strength and stiffness. This is an outcome for the use of composite materials in field of aircraft and space shuttles. In an attempt to develop heat resistant materials FGMs are developed. Composition of two or materials and structures changes over volume by using some gradation laws such as, exponential law power law, stepwise variation and continuous variation [1].

2.2 Functionally Graded Materials

Schmauder et al. [2] investigated mechanical behaviour of ZrO_2/NiCr 80 20 compositions FGMs are analysed and compared with experimental results. And also found that new parameter matricity controls the stress level of composite, globally and also locally. Sladek et al. [3] analysed time dependent heat conduction in nonhomogeneous FGMs. Laplace transforms technique is used to solve initial boundary value problem. Results obtained for finite strip and hollow cylinder having exponential variation of material properties. Shao et al. [4] presented stress analysis of FG hollow circular cylinder in combined mechanical and thermal environment by considering linearly increasing temperature. Temperature dependent material properties are considered and solution for ordinary differential equations are solved by Laplace transforms technique. Farhatnia et al. [5] presented stress distribution for composite beam having FGM in middle layer. Temperature dependent material properties are considered for uniform temperature gradient. Jyothula et al. [6] presented nonlinear analysis of FGMs in thermal environment by changing material variation parameter, aspect ratio, and boundary condition re analysed with higher order displacement model. Nonlinear simultaneous equation are obtained by Navier's method and equations are solved by Newton Raphson iterative method. Callioglu [7] presented thermoelasticity solution for FG disc. By using infinitesimal deformation theory and power law distribution used to get solution. Stress

and displacement variation are presented along radial position due to centrifugal action, steady state temperature, internal and external pressure. Abotula et al. [8] studied stress field for curving cracks in FGMs for thermo-mechanical loading. Using strain energy density criterion effect of curvature parameters, temperature gradients on crack growth directions, non-homogeneity values are found and discussed. Bhandari et al. [9] studied parametric study of FGM plate by varying volume fraction distribution and boundary conditions. Static analysis of FGM plate has studied by sigmoid law and compared with literature. Kursun et al. [10] presented stress distribution in a long hollow FG cylinder under thermomechanical environment. By using infinitesimal deformation theory, solution for displacement model are found.

2.3 Stresses in FGMs

Woo et al. [11] reveals effect of thermomechanical coupling in FGMs plays an important role. Using von Karman theory, fundamental equation for shallow shells are obtained. Material properties and thermomechanical stress field are determined. Reddy and Cheng [12] studied thermomechanical deformation of FG simply supported plates, properties of material are valued by Mori-Tanaka scheme. Temperature, displacement and stress distribution are computed for different volume fraction. Jin and Paulino [13] studied edge crack in a FGM strip under thermal environment. Thermal properties of FGM vary over thickness direction, Young's modulus and Poisson's ratio are assumed to be constant. Temperature solutions are obtained for short time by using Laplace transform and asymptotic analysis. Chakraborty et al. [14] examined stress variation in FGMs by use of both power law and exponential variation of material properties. New beam element is developed for behavioural study of FGMs. Senthil et al [15] presented thermomechanical deformation of a simply supported FG plate subjected to thermal loads on its top and bottom surfaces. Transient displacement and thermal stresses are obtained for several critical location of plate subjected to time dependent temperature and heat flux. Wang et al. [16] developed meshless algorithm to simulate thermal stress distribution in two-dimensional FGMs. Displacement components are determined by governing equations and boundary condition. Tahani et al. [17] presented dynamic characteristics of FG thick hollow cylinder under loading. Temperature dependent material properties are considered and vary long radial direction. Dynamic behaviour of thermo elastic stresses are discussed for various grading index. Gupta et al. [18] studied dynamic crack growth behaviour of FGMs under transient thermo-mechanical loading.

Principal stress and circumferential stress are discussed and are associated with propagating crack tip.

2.4 Rotor Dynamics

Zorzi and Nelson [19] studied damped rotor stability including hysteric and internal viscous damping using linear finite element concept. Rouch and Kao [21] presented cubic function for mass, stiffness and gyroscopic matrices for a beam element used for transverse displacement. Kim and Bert [22] presented critical speed of hollow cylindrical shaft for laminated composite materials using thin and thick shell theories. Obtained results are compared with classical beam theory, results are well accurate. Bert and Kim [23] presents buckling torque for cylindrical hollow laminated composite shaft material. Obtained results are compared with experiments, results are well accurate. Dimarogonas [24] reviewed vibration response for cracked structural member. Based on vibration amplitude and speed of rotation, crack will open and close. Singh and Gupta [25] presented dynamic analysis of composite rotor applying layerwise beam theory and conventional equivalent modulus beam theory. Wettergren and Olsson [26] studied instabilities of horizontal rotor supported on flexible bearings. Found that critical speed can be reduced significantly by internal damping. Abduljabbar et al. [27] presented dynamic vibration control of flexible rotor mounted on journal bearing by using feedback controller device and feed forward controller device. Reddy and Chin [28] studied thermoelastic response of FG cylinders and plates in dynamic in condition. First order shear deformation plate theory is used for transverse shear strains, coupled with heat conduction equation. Liew et al. [29] analysed thermomechanical behaviour of FG cylinders. Solutions are achieved by novel limiting process. Lin et al. [30] presents sensitivity analysis, dynamic behaviour of high speed spindle in thermo-mechanical environment. Spindle stiffness is determined for different speed effect, appropriate cooling effect and bearing preload. Chang et al. [31] studied laminated composite spinning shaft using first order shear deformation theory. Governing equation for rotor derived by employing Hamilton's principle. Shokrieh et al. [32] analysed torsional stability for rotating composite shaft. Effect of stacking sequence and boundary conditions on strength and buckling torque of composite drive shaft has been calculated using finite element analysis. Shao [33] presented solution for displacement, temperature, thermal and mechanical stresses for FG circular hollow cylinder using multi-layered method based on laminated composites model. Temperature dependent material

properties are assumed along radial direction and equal in each layer. Shao and Ma [34] studied stress analysis in FG hollow cylinder subjected to coupled thermal and mechanical environment for linearly varying temperature field. Applying Laplace transform technique, solution for time dependent temperature field and thermo mechanical stress variation has been calculated. Das et al. [35] studied vibration control of transverse vibration of rotor shaft system due to unbalance. Vibration control is done by electromagnets. Xiang and Yang [36] studied free and forced vibration of laminated FG beam of variable thickness for thermally induced stresses using TBT. Roy et al. [37] studied dynamic behaviour of viscoelastic rotor shaft system introducing internal damping of material. Critical speed of rotor can be increased by introducing composite material, aluminium matrix with carbon fibre. Bayat et al. [38] presented thermo elastic analysis for FG rotating disks. Temperature dependent material properties are considered along radial direction with variable thickness of disk. Badie et al. [39] examines natural frequency, buckling strength, failure modes, torsional stiffness and fatigue life of composite drive shaft by changing fibre stacking angle and orientation angle using finite element analysis (FEA). Poursaeidi and Yazdi [40] presented causes of extreme bends in rotor shaft and straightening methods by choosing hot spotting process. Sheihlou et al. [41] studied torsional vibration of FG micro-shaft using Hamilton's principle. Vibrations equations are solved by Galerkin's weighted residual technique. Also studied effect of volume fraction and boundary condition on natural frequency and frequency response of micro FG shaft. Rao et al. [42] analysed dynamic behaviour of FG shaft using TBT. Material properties are assumed to be vary according to exponential law.

2.5 Motivation

Though literature review discloses a lot of research work has been done on thermo mechanical stress analysis of composites and FGMs. Research on stress analysis of FG tapered shaft system based on TBT has not been yet discussed. Considering shaft rotating in high temperature environment like turbine shaft, rocket engine components FGMs gives better solution over traditional composite materials. Stress distribution in tapered FG shaft under thermal and mechanical environment compared with traditional materials. Present work discloses stress analysis of rotor shaft system with FGMs under both thermal and mechanical environment.

2.6 Aim of Present Work

Main objectives of present work has been laid down here,

i. Material modelling for tapered FG shaft based on power law gradation.
ii. Modelling of temperature dependent material properties for FG shaft.
iii. Variation of mechanical properties with respect to temperature and power law indexes along radial direction.
iv. To study stresses developed in tapered shafts made of FGMs.
v. Comparative study between tapered FG shaft and tapered Stainless Steel shaft.
vi. To study the stresses developed both in thermal and mechanical environment for different speed, varying power law index value.

CHAPTER 3

MATERIAL MODELLING FOR TAPERED FG SHAFT

Material modelling of FG tapered shaft is explained in detail in this chapter by taking power law gradation and exponential gradation.

3.1 Actual Material Properties of FGM

Properties of FGMs are changing along certain directions, so that it is required to find effective material properties of FGMs applying to shaft. For exact analysis of FGMs it is required to find accurate material properties. Many simulations are established for determining properties of FG shaft. Bulk constituent properties assumes no interaction between phases by employing rule of mixture. Thermo physical properties are derived by variational approach. Spatial distribution of constituent materials are having information about micromechanical approach.

3.2 Material Modelling of FGMs

Considering FG beam of finite length and thickness, made of Aluminum Oxide (Al_2O_3) as a ceramic material and Stainless Steel (SUS304) as a metal. Here material are varying along y direction, treating top $\left(y=+\frac{h}{2}\right)$ surface as ceramic and bottom $\left(y=-\frac{h}{2}\right)$ surface as metal. Considering P as an actual material properties,

$$P = P_m V_m + P_c V_c \tag{1}$$

Where P_m, V_m and P_c, V_c are material properties, volume fraction of metal and ceramic respectively. Also sum of volume fraction of metal (V_m) and volume fraction of ceramic (V_c) are always unity at any graded direction. It is related as,

$$V_m + V_c = 1 \tag{2}$$

3.2.1 Laws of Gradation

There are many laws for varying volume fraction of materials namely, power law gradation, exponential law of gradation, step wise gradation and continuous gradation etc. Mainly researchers are using power law gradation and exponential law.

3.2.1.1 Power Law Gradation

Here volume fraction of materials changes along certain direction, by using index called as power law index *k*. This factor controls volume fraction of any materials and controls shape, strength of material. Figure 3. 1 shows volume fraction of metal in FGMS. This is expressed for rectangular block as,

$$V_c(y) = \left(\frac{2y+h}{2h}\right)^k \tag{3}$$

Where $k \geq 0$

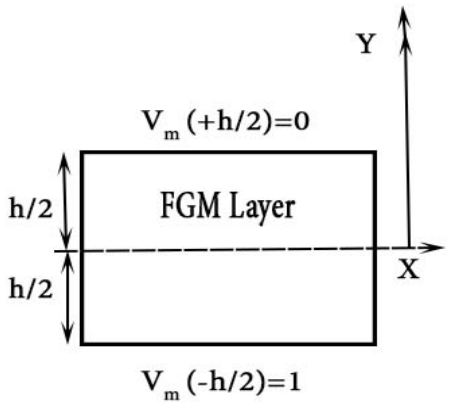

Figure 3. 1 Volume fraction of metal in FGM rectangular cross-section.

If p is temperature dependent material properties, it can be written as,

$$P = P_0\left(P_{-1}\theta^{-1} + 1 + P_1\theta + P_2\theta^2 + P_3\theta^3\right) \tag{4}$$

Where P_{-1}, P_1, P_2 and P_3 are temperature coefficients θ^{-1}, θ^1, θ^2 and θ^3 respectively and P_0 material properties at ambient temperature. Here material properties are function of temperature and certain direction and it is given by,

$$E(y,\theta)=\left\{E_c(\theta)-E_m(\theta)\right\}\left(\frac{2y+h}{2h}\right)^k+E_m(\theta)$$
$$\nu(y,\theta)=\left\{\nu_c(\theta)-\nu_m(\theta)\right\}\left(\frac{2y+h}{2h}\right)^k+\nu_m(\theta)$$
$$\alpha(y,\theta)=\left\{\alpha_c(\theta)-\alpha_m(\theta)\right\}\left(\frac{2y+h}{2h}\right)^k+\alpha_m(\theta) \quad (5)$$
$$\rho(y)=(\rho_c-\rho_m)\left(\frac{2y+h}{2h}\right)^k+\rho_m$$

Density is assumed to be not dependent on temperature and it is vary along certain directions only.

3.2.1.2 Exponential Law of Gradation

In this gradation material properties are vary along certain directions as,

$$P(y)=P_0e^{k\left(y+\frac{h}{2}\right)} \quad (6)$$

Where P_0 denotes, bottom surface material properties of FGM, 'k' is the factor which controls gradation across thickness 'h'. Young's modulus thermal conductivity, coefficient of thermal expansion and density of the FG material are given as,

$$E(y)=E_0e^{k\left(y+\frac{h}{2}\right)} \qquad \alpha(y)=\alpha_0e^{k\left(y+\frac{h}{2}\right)} \quad (7)$$

$$K(y)=K_0e^{k\left(y+\frac{h}{2}\right)} \qquad \rho(y)=\rho_0e^{k\left(y+\frac{h}{2}\right)} \quad (8)$$

This simple rule of mixture is assumes poison's ratio is constant.

3.3 Modelling of Material Properties Applicable To tapered FG Shaft

Tapered shaft with finite length *L*, inner radius at beginning and end of shaft are R_0 and R_1 respectively having constant thickness of t throughout the tapered shaft. Top surface of shaft is of ceramic rich and inner surface of shaft is metal rich.

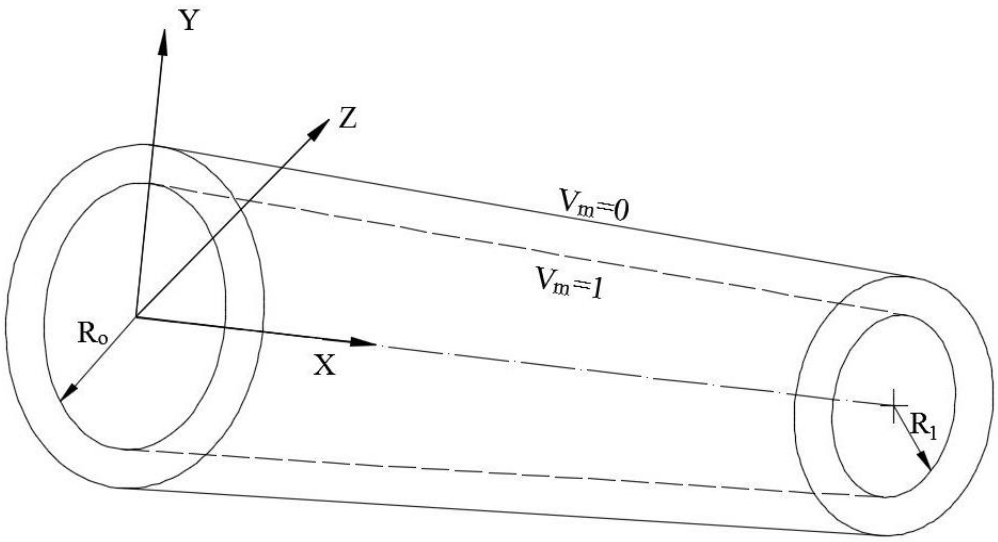

Figure 3. 2 Volume fraction of metal in tapered FG shaft

3.3.1 Power Law

Figure 3. 2 Volume fraction of metal in tapered FG shaft across the radius of tapered shaft, it is considered as Two Dimensional variation. FG rotating shaft is a composed of Stainless steel (SUS3O4) and Aluminum oxide (Al_2O_3) as metal and ceramic materials. Volume fraction of these materials are varied along Y direction using power law and gradation factor k. Here radius of shaft is a function in x as radius is going to change along x direction. Volume fraction for ceramic is given by,

$$V_c(y) = \left(\frac{r - r_m}{r_c - r_m}\right)^k \tag{9}$$

Where, $k \geq 0$

Here, sum of volume fraction of metal and ceramic is unity at any particular radius of shaft i.e.

$$V_m + V_c = 1 \tag{10}$$

Let *'P'* be temperature dependent material properties and it can be written as,

$$P = P_0\left(P_{-1}\theta^{-1} + 1 + P_1\theta + P_2\theta^2 + P_3\theta^3\right) \tag{12}$$

Where P_{-1}, P_1, P_2 and P_3 are temperature coefficients θ^{-1}, θ^1, θ^2 and θ^3 respectively and P_0 material properties at ambient temperature. Here material properties are function of temperature and certain direction and it is given by,

$$
\begin{aligned}
E(y,\theta) &= \left\{E_c(\theta) - E_m(\theta)\right\}\left(\frac{r-r_m}{r_c-r_m}\right)^k + E_m(\theta)\\
\nu(y,\theta) &= \left\{\nu_c(\theta) - \nu_m(\theta)\right\}\left(\frac{r-r_m}{r_c-r_m}\right)^k + \nu_m(\theta)\\
\alpha(y,\theta) &= \left\{\alpha_c(\theta) - \alpha_m(\theta)\right\}\left(\frac{r-r_m}{r_c-r_m}\right)^k + \alpha_m(\theta)\\
\rho(y) &= (\rho_c - \rho_m)\left(\frac{r-r_m}{r_c-r_m}\right)^k + \rho_m
\end{aligned}
\tag{13}
$$

Density is assumed to be not dependent on temperature and it is vary along certain directions only. One Dimensional steady state temperature field is assumed by Fourier heat conduction equation without considering heat generation is given by,

$$
\frac{d}{dy}\left[K(y)\frac{d\theta}{dy}\right] = 0; \quad \theta = \theta_c \quad at \quad y = r_c; \quad \theta = \theta_m \quad at \quad y = r_m
$$

Where θ_m and θ_c are the temperatures in metal-rich and ceramic-rich surfaces respectively. The temperature variation is assumed to occur in the radial direction only, and the temperature field is assumed by considering the following polynomial series [43]

$$
\theta(y) = \theta_m + (\theta_c - \theta_m)\zeta(y) \tag{14}
$$

Where

$$
\zeta(y) = \frac{1}{C}\left[\begin{aligned}
&(\bar{r}) - \frac{K_{cm}}{(k+1)K_m}(\bar{r})^{k+1} + \frac{K^2{}_{cm}}{(2k+1)K^2{}_m}(\bar{r})^{2k+1} - \frac{K^3{}_{cm}}{(3k+1)K^3{}_m}(\bar{r})^{3k+1}\\
&+ \frac{K^4{}_{cm}}{(4k+1)K^4{}_m}(\bar{r})^{4k+1} - \frac{K^5{}_{cm}}{(5k+1)K^5{}_m}(\bar{r})^{5k+1}
\end{aligned}\right]
$$

Where $K_{cm} = K_c - K_m$, $\bar{r} = \left(\frac{r-r_m}{r_c-r_m}\right)$ and

$$
C = \left[1 - \frac{K_{cm}}{(k+1)K_m} + \frac{K^2{}_{cm}}{(2k+1)K^2{}_m} - \frac{K^3{}_{cm}}{(3k+1)K^3{}_m} + \frac{K^4{}_{cm}}{(4k+1)K^4{}_m} - \frac{K^5{}_{cm}}{(5k+1)K^5{}_m}\right]
$$

CHAPTER 4

FORMULATION FOR TAPERED FG SHAFT

4.1 Introduction

FG tapered shaft consists of three nodded Timoshenko beam, based on the First order shear deformation theory considering both Gyroscopic and rotary inertia effect. Hollow circular cross section shaft is considered for analysis and it is rotating about its longitudinal axis. Figure 4. 1 shows displacement variables and Figure 4. 2 shows diagram representing the shaft.

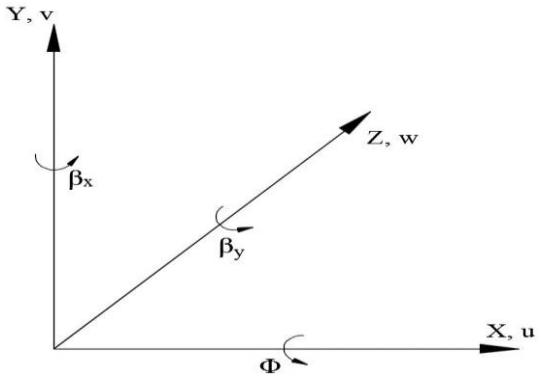

Figure 4. 1 Displacement variables

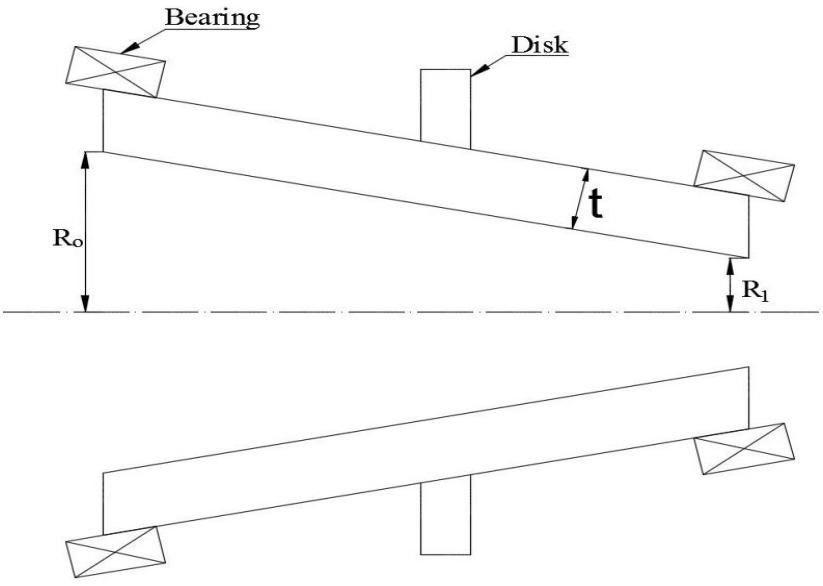

Figure 4. 2 Diagram showing tapered shaft and bearing system

4.2 Finite Element Modelling of Shaft

FG rotating shaft has modelled using Finite element method for three nodded Timoshenko beam element having six degrees of freedom at each node. By applying linear elastic and small deflection theory is assumed in present work.

Assumed displacement field as given below [31],

$$\left.\begin{aligned} u_x(x,y,z,t) &= u(x,t) + z\beta_x(x,t) - y\beta_y(x,t) \\ u_y(x,y,z,t) &= v(x,t) - z\phi(x,t) \\ u_z(x,y,z,t) &= w(x,t) + y\phi(x,t) \end{aligned}\right\} \tag{15}$$

Strain-displacement relations can be written in Cartesian coordinate system as,

$$\left.\begin{aligned} \varepsilon_{xx} &= \frac{\partial u}{\partial x} + z\frac{\partial \beta_x}{\partial x} - y\frac{\partial \beta_y}{\partial x}; \quad \varepsilon_{xy} = \frac{1}{2}\left(-\beta_y + \frac{\partial v}{\partial x} - z\frac{\partial \phi}{\partial x}\right) \\ \varepsilon_{xz} &= \frac{1}{2}\left(\beta_x + \frac{\partial w}{\partial x} + y\frac{\partial \phi}{\partial x}\right); \quad \varepsilon_{yy} = \varepsilon_{zz} = \varepsilon_{yz} = 0 \end{aligned}\right\} \tag{16}$$

These strain relations can be transformed in to cylindrical coordinate system by using transformation matrix. Strain-displacement relations can now be written in cylindrical coordinate system by taking $y = r\,cos\theta$, $z = r\,sin\theta$, $m = cos\theta$ and $n = sin\theta$.

$$\begin{bmatrix} \varepsilon_{xx} \\ \varepsilon_{x\theta} \\ \varepsilon_{xr} \end{bmatrix} = \begin{bmatrix} 1 & 0 & 0 \\ 0 & -n & m \\ 0 & m & n \end{bmatrix} \begin{Bmatrix} \varepsilon_{xx} \\ \varepsilon_{xy} \\ \varepsilon_{xz} \end{Bmatrix} \tag{17}$$

Where

$$\left.\begin{aligned} \varepsilon_{xx} &= \frac{\partial u}{\partial x} + r\sin\theta\frac{\partial \beta_x}{\partial x} - r\cos\theta\frac{\partial \beta_y}{\partial x}; \quad \varepsilon_{rr} = \varepsilon_{\theta\theta} = \varepsilon_{r\theta} = 0 \\ \varepsilon_{x\theta} &= \frac{1}{2}\left(\beta_y\sin\theta + \beta_x\cos\theta - \sin\theta\frac{\partial v}{\partial x} + \cos\theta\frac{\partial w}{\partial x} + r\frac{\partial \phi}{\partial x}\right) \\ \varepsilon_{xr} &= \frac{1}{2}\left(\beta_x\sin\theta - \beta_y\cos\theta + \sin\theta\frac{\partial w}{\partial x} + \cos\theta\frac{\partial v}{\partial x}\right) \end{aligned}\right\} \tag{18}$$

And the above strain displacement relations in cylindrical coordinate can be written in matrix form as,

$$\begin{bmatrix}\varepsilon_{xx}\\ \gamma_{x\theta}\\ \gamma_{xr}\end{bmatrix}=\frac{1}{2}\begin{bmatrix}2\frac{\partial}{\partial x} & 0 & 0 & 2r\sin\theta\frac{\partial}{\partial x} & -2r\cos\theta\frac{\partial}{\partial x} & 0\\ 0 & -\sin\theta\frac{\partial}{\partial x} & \cos\theta\frac{\partial}{\partial x} & \cos\theta & \sin\theta & r\frac{\partial}{\partial x}\\ 0 & \cos\theta\frac{\partial}{\partial x} & \sin\theta\frac{\partial}{\partial x} & \sin\theta & -\cos\theta & 0\end{bmatrix}\begin{Bmatrix}u\\ v\\ w\\ \beta_x\\ \beta_y\\ \phi\end{Bmatrix} \tag{19}$$

Stress strain relations in any layer of the FG shaft can be written as [31],

$$\begin{bmatrix}\sigma_{xx}\\ \tau_{x\theta}\\ \tau_{xr}\end{bmatrix}=\begin{bmatrix}C_{11r} & k_sC_{16r} & 0\\ k_sC_{16r} & k_sC_{66r} & 0\\ 0 & 0 & k_sC_{55r}\end{bmatrix}\begin{Bmatrix}\varepsilon_{xx}\\ \gamma_{x\theta}\\ \gamma_{xr}\end{Bmatrix} \tag{20}$$

Where k_s is the shear correction factor and C_{ijr} represents constitutive element, related to elastic constants for transversely isotropic material.

Coupled (thermo-mechanical) stress strain relations in any layer of FG shaft can be written as,

$$\begin{bmatrix}\sigma_{xx}\\ \tau_{x\theta}\\ \tau_{xr}\end{bmatrix}=\begin{bmatrix}C_{11r} & k_sC_{16r} & 0\\ k_sC_{16r} & k_sC_{66r} & 0\\ 0 & 0 & k_sC_{55r}\end{bmatrix}\left\{\begin{bmatrix}\varepsilon_{xx}\\ \gamma_{x\theta}\\ \gamma_{xr}\end{bmatrix}-\begin{bmatrix}\alpha\Delta T\\ 0\\ 0\end{bmatrix}\right\} \tag{21}$$

4.2.1 Kinetic Energy Expression of Shaft

The effect of both rotary and translation of FG shaft are considered for deriving kinetic energy expression, it is written as,

$$T_s=\frac{1}{2}\int_0^L\begin{bmatrix}I_m(\dot{u}^2+\dot{v}^2+\dot{w}^2)+I_d(\dot{\beta}_x{}^2+\dot{\beta}_y{}^2)-2\Omega I_p\beta_x\dot{\beta}_y\\ +I_p\dot{\phi}^2+2\Omega I_p\dot{\phi}+\Omega^2I_p+\Omega^2\,\mathrm{I}_d(\beta_x{}^2+\beta_y{}^2)\end{bmatrix}dx \tag{22}$$

Where,

Ω is rotating speed of the shaft, L is length of the shaft, I_p, I_m and I_d are polar mass moment of inertia, mass moment of inertia and diametrical mass moment of inertia respectively. In above equation neglecting some small terms, first variation of kinetic energy is written as,

$$\delta T_s = \int_0^L \left[\begin{array}{l} I_m \left(\dot{u} \dfrac{\partial \delta u}{\delta t} + \dot{v} \dfrac{\partial \delta v}{\delta t} + \dot{w} \dfrac{\partial \delta w}{\delta t} \right) + I_d \left(\dot{\beta}_x \dfrac{\partial \delta \beta_x}{\delta t} + \dot{\beta}_y \dfrac{\partial \delta \beta_y}{\delta t} \right) \\ + I_p \dot{\phi} \delta \dot{\phi} + \Omega I_p \delta \dot{\phi} - \Omega \, \mathrm{I}_d \left(\beta_x \dfrac{\partial \delta \beta_y}{\delta t} + \dot{\beta}_y \delta \beta_x \right) \end{array} \right] dx \tag{23}$$

4.2.2 Strain Energy Equation for FG Shaft

Strain energy of FG shaft is given by,

$$U_s = \frac{1}{2} \int_V [\sigma]^T [\varepsilon] dV = \frac{1}{2} \int_V \left(\sigma_{xx} \varepsilon_{xx} + \sigma_{rr} \varepsilon_{rr} + \sigma_{\theta\theta} \varepsilon_{\theta\theta} + 2\tau_{xr} \varepsilon_{xr} + 2\tau_{x\theta} \varepsilon_{x\theta} + 2\tau_{r\theta} \varepsilon_{r\theta} \right) dV \tag{24}$$

As $\varepsilon_{rr} = \varepsilon_{\theta\theta} = \varepsilon_{r\theta} = 0$

Strain energy can be rewritten as,

$$U_s = \frac{1}{2} \int_V (\sigma_{xx} \varepsilon_{xx} + 2\tau_{xr} \varepsilon_{xr} + 2\tau_{x\theta} \varepsilon_{x\theta}) dV \tag{25}$$

By taking variation in strain energy expression we get,

$$\delta U_s = \int_V \left(\begin{array}{l} \sigma_{xx} \left(\dfrac{\partial u}{\partial x} + r \sin\theta \dfrac{\partial \beta_x}{\partial x} - \right. \\ \left. r \cos\theta \dfrac{\partial \beta_y}{\partial x} \right) + \tau_{xr} \left(\begin{array}{l} \beta_x \sin\theta - \beta_y \cos\theta + \\ \sin\theta \dfrac{\partial w}{\partial x} + \cos\theta \dfrac{\partial v}{\partial x} \end{array} \right) + \\ \tau_{x\theta} \left(\beta_y \sin\theta + \beta_x \cos\theta - \sin\theta \dfrac{\partial v}{\partial x} + \cos\theta \dfrac{\partial w}{\partial x} + r \dfrac{\partial \phi}{\partial x} \right) \end{array} \right) dV \tag{26}$$

Where, $dV = r d\theta dr dx$

4.2.3 Kinetic energy expression for disks on shaft

Disks fixed on shaft are treated as isotropic material. Expression for kinetic energy of disks is written as,

$$T_d = \frac{1}{2} \int_0^L \sum_{i=1}^{N_D} \left[\begin{array}{l} I_{mi}^D \left(\dot{u}^2 + \dot{v}^2 + \dot{w}^2 \right) + I_{di}^D \left(\dot{\beta}_x{}^2 + \dot{\beta}_y{}^2 \right) \\ -2\Omega I_{di}^D \beta_x \dot{\beta}_y + I_{pi}^D \dot{\phi}^2 + 2\Omega I_{pi}^D \dot{\phi} + \Omega^2 I_{pi}^D \end{array} \right] \Delta(x - x_{Di}) dx \tag{27}$$

Where I_{mi}^{D}, I_{di}^{D} and I_{pi}^{D} mass moment of inertia, diametrical and polar mass moment of inertia of i^{th} disk respectively. The term $\Delta\left(x-x_{Di}\right)$ represents one dimensional spatial Dirac delta function. x_{Di} gives location i^{th} disk and N_{D} is the number of disks which are attached to shaft. Variation of the kinetic energy of disk given by,

$$\delta T_d = \int_0^L \sum_{i=1}^{N_D} \begin{bmatrix} I_{mi}^{D}\left(\dot{u}\dfrac{\partial\delta u}{\delta t}+\dot{v}\dfrac{\partial\delta v}{\delta t}+\dot{w}\dfrac{\partial\delta w}{\delta t}\right)+I_{di}^{D}\left(\dot{\beta}_x\dfrac{\partial\delta\beta_x}{\delta t}+\dot{\beta}_y\dfrac{\partial\delta\beta_y}{\delta t}\right)- \\ \Omega I_{pi}^{D}\left(\dot{\beta}_y\delta\beta_x+\beta_x\dfrac{\partial\delta\beta_y}{\delta t}\right)+I_{pi}^{D}\dot{\phi}\delta\dot{\phi}+I_{pi}^{D}\Omega\delta\dot{\phi} \end{bmatrix}\Delta(x-x_{Di})dx \qquad (28)$$

4.3 Expression for work done to external load and bearings

R_{x}, R_{y} and R_{z} are external force intensities, M_{x}, M_{y} and $M_{\text{x}\theta}$ are external intensities of moments distributed along shaft length. Virtual work done by external loads is given by,

$$\delta W_e = \int_0^L \left(R_x\delta u+R_y\delta v+R_z\delta w+M_y\delta\beta_y+M_x\delta\beta_x+M_{x\theta}\delta\phi\right)dx \qquad (29)$$

Spring and viscous damper bearing are modelled here and virtual work done by springs and dampers are given by,

$$\delta W_B = \int_0^L \sum_{i=1}^{N_B} \begin{bmatrix} -K_{yy}^{Bi}v\delta v-K_{zy}^{Bi}v\delta w-K_{yz}^{Bi}w\delta v-K_{zz}^{Bi}w\delta w \\ -C_{yy}^{Bi}\dot{v}\delta\dot{v}-C_{zy}^{Bi}\dot{v}\delta\dot{w}-C_{yz}^{Bi}\dot{w}\delta\dot{v}-C_{zz}^{Bi}\dot{w}\delta\dot{w} \end{bmatrix}\Delta(x-x_{Bi})dx \qquad (30)$$

Where K^{Bi} and C^{Bi} represents equivalent stiffness and equivalent damping coefficient of i^{th} bearing.

4.4 Governing equation of rotor shaft

The governing equation of rotating shaft can be derived by using above strain energy expression, kinetic energy of shaft and disks, work done expressions by external loads and bearings by applying Hamilton's principle. Which is given by,

$$\int_{t1}^{t2}\left[\delta T-\delta U_s+\delta W_e+\delta W_B\right]dt=0 \qquad (31)$$

Total kinetic energy of shaft and disks is given by $T=T_s+T_d$

$$\int_{t1}^{t2}\left[\delta\left(T_s+T_d\right)-\delta U_s+\delta W_e+\delta W_B\right]dt=0 \tag{32}$$

Finite element analysis is to find field variables at each nodal points by approximate analysis, taking nodes within the elements. These variables is a function of values at nodal points of the element, this function is called as interpolation function or shape function. In present model three node one dimensional Timoshenko beam element is considered having six degrees of freedom at each node.

Lagrangian interpolation function is used to approximate the displacement fields rotating shaft. Elemental nodal degree of freedom at each node are u, v, w, β_x, β_y, ϕ. Displacement field variables are given by,

$$\begin{aligned} u&=\sum_{k=1}^{r}u^k(t)\psi_k(\eta); \quad v=\sum_{k=1}^{r}v^k(t)\psi_k(\eta); \quad w=\sum_{k=1}^{r}w^k(t)\psi_k(\eta)\\ \beta_x&=\sum_{k=1}^{r}\beta_x^k(t)\psi_k(\eta); \quad \beta_y=\sum_{k=1}^{r}\beta_y^k(t)\psi_k(\eta); \quad \phi=\sum_{k=1}^{r}\phi^k(t)\psi_k(\eta)\end{aligned} \tag{33}$$

One dimensional Lagrangian polynomial is given by,

$$L_k(\eta)=\prod_{\substack{m=1\\ m\neq k}}^{r}\frac{\eta-\eta_m}{\eta_k-\eta_m}$$

Above equation gives value zero at all points except k = 1, L_k is Lagrangian polynomial and ψ_k (k = 1, 2, 3…) interpolation function and η is the natural coordinate whose value varies from -1 to +1. For three node element r is equal to three, shape function can be written as,

$$\psi_1=\frac{-\eta(1-\eta)}{2};\ \psi_2=1-\eta^2;\quad \psi_3=\frac{\eta(1+\eta)}{2} \tag{34}$$

Now by putting above displacement variables into the governing equations we get following equation of motion for FG spinning shaft.

$$[M]\{\ddot{q}\}+\left([C]+\Omega[G]\right)\{\dot{q}\}+[K]\{q\}=\{F\} \tag{35}$$

Where [M] is mass matrix, [G] is gyroscopic matrix, [C] is total damping matrix, [K] is structural stiffness matrix, {q} is nodal displacement vector and {F} is the external force vector.

4.5 Contribution of internal damping

By including both internal viscous and hysteresis damping [19] of shaft and disk elements extended final equation of motion can written as,

$$[M]\{\ddot{q}\}+\left([C]+\Omega[G]+\eta_V[K]\right)\{\dot{q}\}+\left[\begin{array}{l}\left(\frac{1+\eta_H}{\sqrt{1+\eta_H^2}}\right)[K]+\\ \left(\eta_V\Omega+\frac{\eta_H}{\sqrt{1+\eta_H^2}}\right)[K_{cir}]\end{array}\right]\{q\}=\{F\} \tag{36}$$

Where K_{cir} is the skew-symmetric circulation matrix [16].

CHAPTER 5

RESULTS AND DISCUSSION

A complete MATLAB code has been developed and validated for above formulation. Results are presented for different stresses, speed and power law index value based on problem specified below.

5.1 Problem Description and Summarization of Discussion

Tapered shaft consists of rigid disk attached at its centre, supported on two similar bearings. Shaft is modelled for present analysis using three nodded beam element. Dimensions of shaft and rigid disk are presented in Table 5. 1. Tapered shaft is divided into 10 elements, and 8 equal thick layers. Stiffness and damping coefficients for two identical bearings are taken as $K_{yy}=7\times10^{7}$ N/m, $K_{zz}=5\times10^{7}$ N/m, $C_{yy}=700$ Ns/m, $C_{zz}=500$ Ns/m.

Table 5. 1 Geometric dimensions of steel and FG tapered shaft

Parameter	FG Shaft	Disk
Shaft length (*m*)	1.0	
Beginning radius, R_o (*m*)	0.035	
End radius, R_s (*m*)	0.015	
Thickness of hollow shaft, t (*m*)	0.03	
Coefficient of viscous damping (*Ns/m*)	0.0002	
Coefficient of hysteric damping (*Ns/m*)	0.0002	
Density (Kg/m^3)		7800
Outer diameter (*m*)		0.24
Thickness (*mm*)		5.0

Developed MATLAB code has been validated for present available literatures. Several results for FG tapered shaft has presented in this chapter. Primarily, temperature distribution in FG shaft along radial direction is shown for different power law index value. Table 5. 2 and Table 5. 3 are

values for temperature dependent material properties such as young's modulus, Poisson's ratio, coefficient of thermal expansion (CTE) and density of material are plotted along radial direction for different power law index. Next, comparative study between stainless steel shaft and FG shaft. Then, transient stress analysis is carried out for different speed and power law index value.

Table 5. 2 Material properties of FGM [43]

Properties	Stainless Steel	Aluminum oxide
Young's Modulus (*GPa*)	210	390
Poisson's ratio	0.3	0.26
Density	7800	3960

Table 5. 3 Materials and temperature coefficient of mechanical properties [28]

Property	Material	P_0	P_{-1}	P_1	P_2	P_3
E (*Pa*)	SUS304	201.035×10^{9}	0	3.079×10^{-4}	-6.533×10^{-7}	0
	Al_2O_3	349.548×10^{9}	0	-3.853×10^{-4}	4.027×10^{-7}	-1.673×10^{-10}
K (*W/mK*)	SUS304	15.3789	0	-0.00126	0.209×10^{-5}	-7.22×10^{-10}
	Al_2O_3	-14.087	-1123.6	0.00044	0	0
CTE (*1/K*)	SUS304	12.33×10^{-6}	0	0.0008	0	0
	Al_2O_3	6.827×10^{-5}	0	0.00018	0	0
Poisson Ratio	SUS304	0.3262	0	-2.001×10^{-4}	3.797×10^{-7}	0
	Al_2O_3	0.26	0	0	0	0

5.2 Validation of Code

To verify the developed code, uniform shaft made of graphite epoxy composite material with disk at centre of shaft [31] (dimensions are in Table 5. 5). Obtained results are well agreement with literature. Figure 5. 1 shows Campbell diagram for first four pairs of modes attained an excellent match with published result [31]. Subsequently temperature dependent material property are discussed, these Figures are also match with already published results, thus developed codes are validated for correctness.

Table 5. 4 Dimensions and properties of laminated graphite-epoxy shaft [35]

Parameters	Composite shaft	Disk	Bearing
Length (*m*)	0.72		
Inner diameter (*m*)	0.028		
Outer diameter (*m*)	0.048		
Shear correction factor	0.56		
Model damping ratio	0.01		
I_m^D (*Kg*)		2.4364	
e (10^{-5} *m*)		5.0	
I_p^D (*Kg* m^2)		0.3778	
I_d^D (*Kg* m^2)		0.1901	
K_{yy}=K_{zz} (10^7 *N/m*)			1.75
C_{yy}=C_{zz} (10^2 *Ns/m*)			5.0

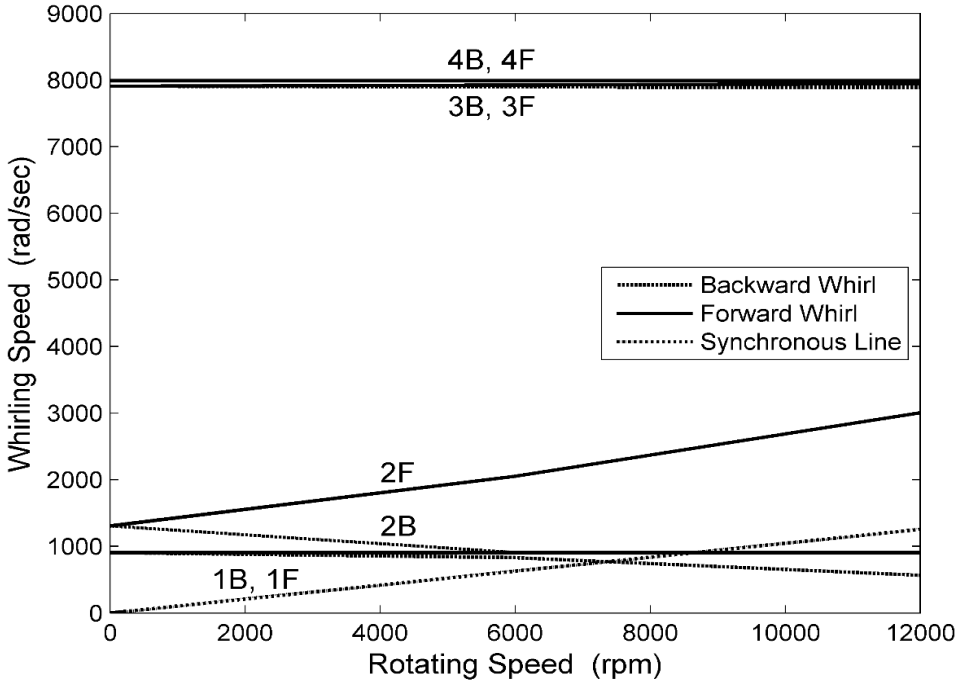

Figure 5. 1 Campbell diagram for laminated graphite-epoxy composite material.

5.3 Temperature Distribution in Tapered FG Shaft

Temperature variation in tapered FG shaft is shown in Figure 5. 2. As material properties are functions of temperature and radial direction, presented here temperature distribution. This variation is due to thermal conductivity, CTE, young's modulus of material. Temperature variation is obtained at mid-section of tapered shaft, it is observed that, for k zero to one temperature decreases gradually and k greater than one temperature increases.

Table 5. 5 Temperature variation in mid-section of tapered FG shaft.

Radius (m)	0.0279	0.0316	0.0354	0.0391	0.0429	0.0466	0.0504	0.0541
k	T_1(K)	T_2(K)	T_3(K)	T_4(K)	T_5(K)	T_6(K)	T_7(K)	T_8(K)
0	471.88	515.63	559.38	603.13	646.88	690.63	734.38	778.13
0.2	469.67	510.19	552.50	595.90	640.15	685.10	730.68	776.81
0.5	468.78	507.56	548.46	591.04	635.11	680.60	727.45	775.60
1	468.82	507.20	547.11	588.66	632.01	677.30	724.73	774.50
5	470.66	511.98	553.32	594.76	636.55	679.24	724.03	773.58
10	471.20	513.60	556.00	598.40	640.82	683.41	726.87	774.48

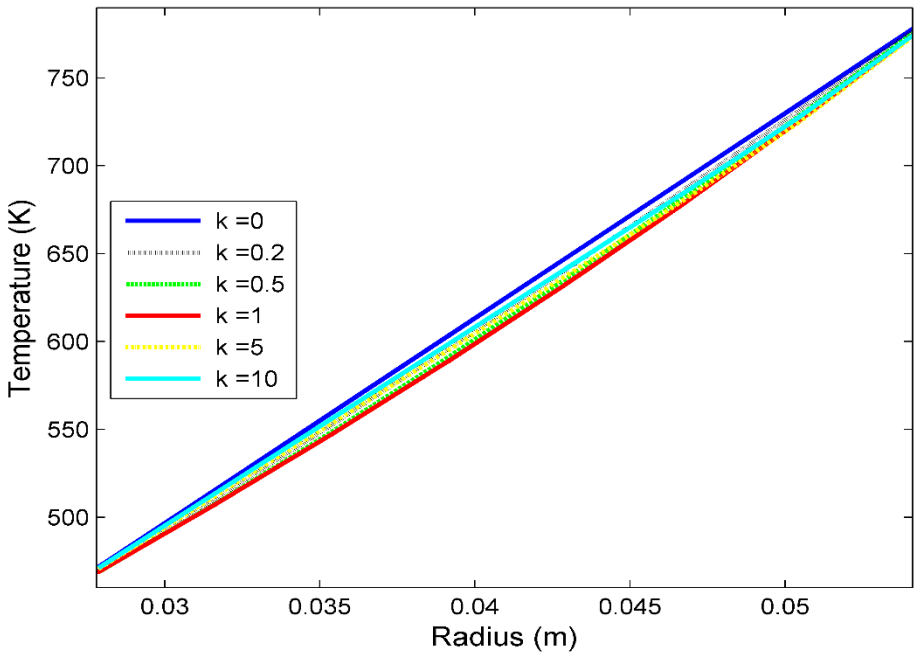

Figure 5. 2 Temperature variation in mid-section of tapered FG shaft.

5.4 Material properties of tapered FG shaft depends on temperature and power law index

Tapered FG shaft is modelled by taking Aluminum oxide as a ceramic and Stainless steel as a metal, these are rich at top and bottom surfaces respectively. Figure 5. 3 shows volume fraction of ceramic material of FGM. Properties of material are changes along radius of shaft, here power law index is significant factor. According to above consideration and formulation, as 'k' value approaches to zero, material becomes fully ceramic and as 'k' value approaches to infinity material becomes fully metal. Linear variation of material is obtained by taking k=1. Since shaft is in thermal environment, it is necessary to find properties depends on temperature. Figure 5. 4 Figure 5. 5 and Figure 5. 6 are modulus elasticity, Poisson's ratio and coefficient of thermal expansion (CTE) respectively. Here properties are changing for each element as analysis is progressed. Also assumed that properties are average of inner and outer surface of a particular layer is at the middle of the layer.

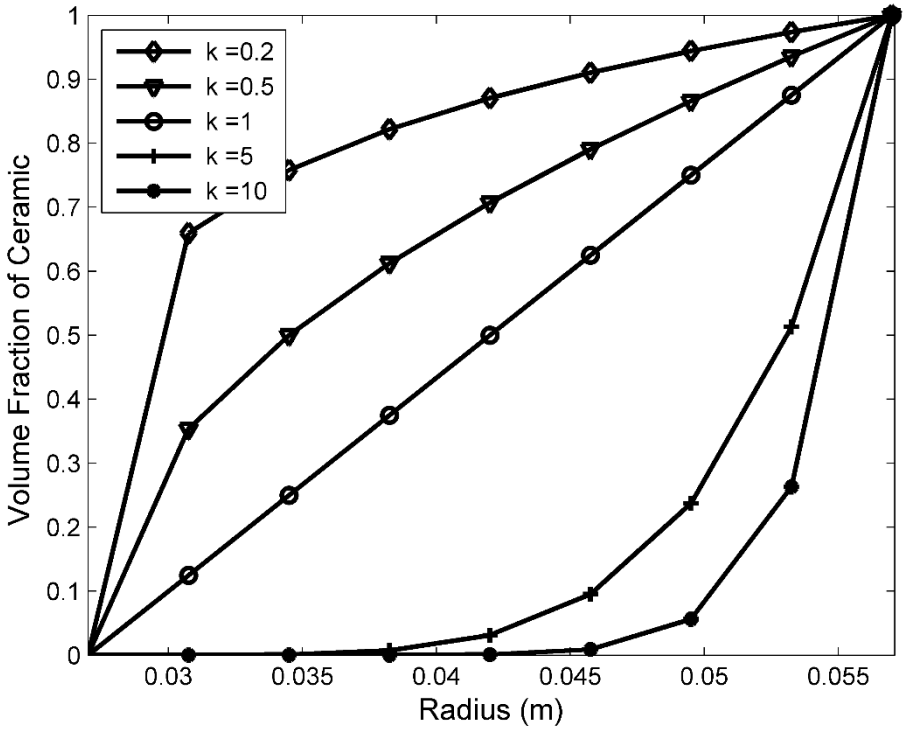

Figure 5. 3 Volume fraction of ceramic material along radius for power law index.

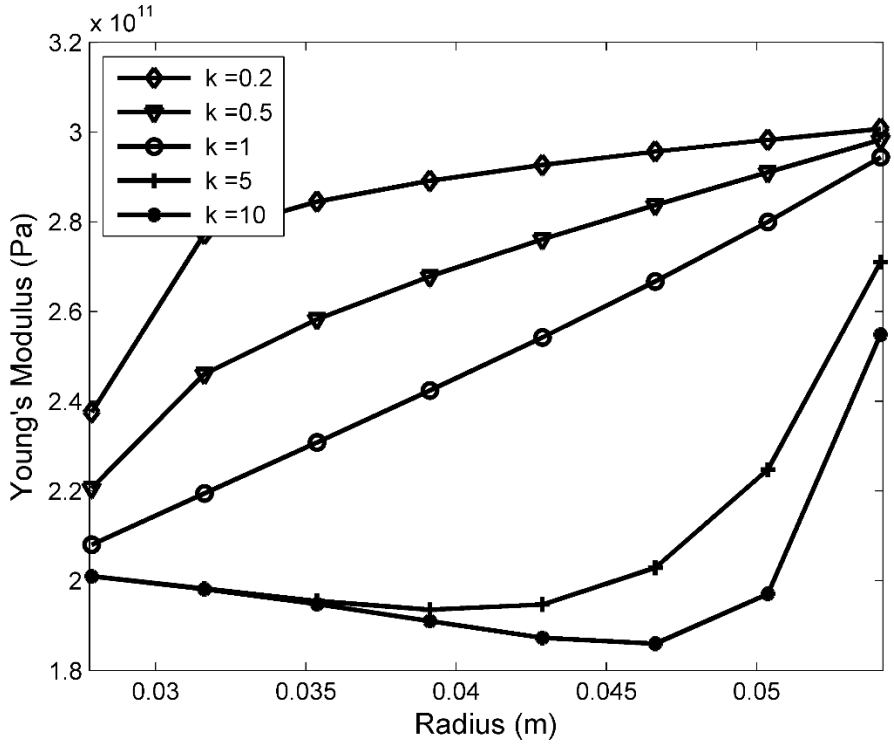

Figure 5. 4 Variation of young's modulus along radius for power law index.

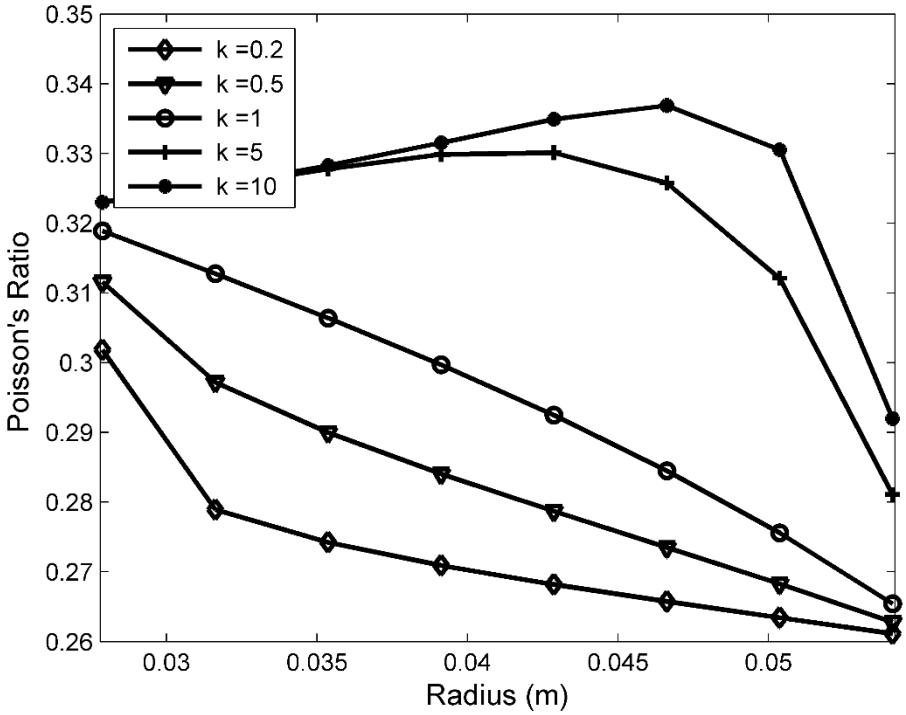

Figure 5. 5 Variation of Poisson's ratio along radius for power law index.

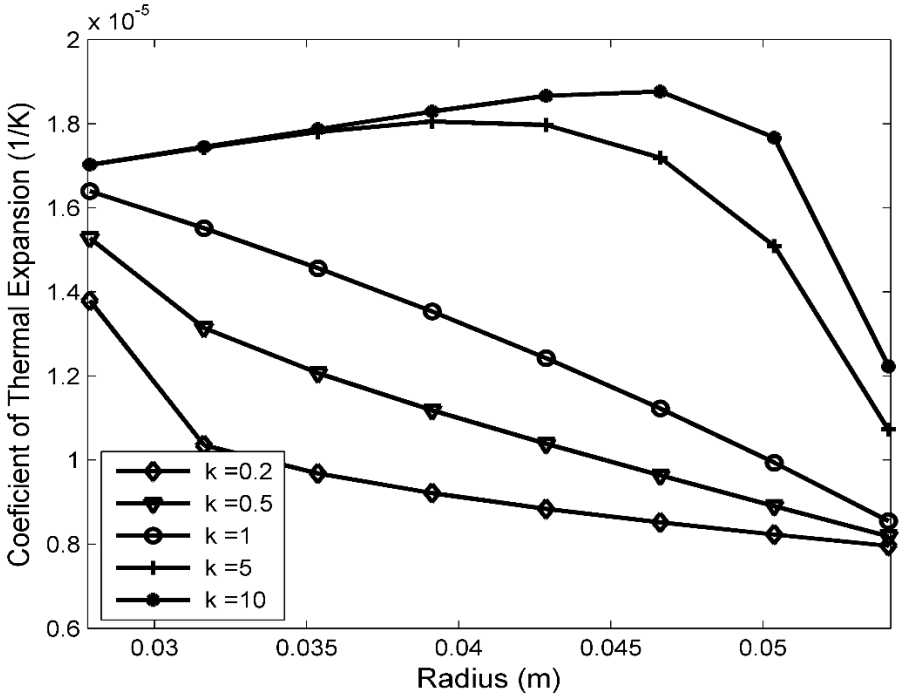

Figure 5. 6 Variation of CTE along radius for power law index.

5.5 Stress analysis in tapered FG shaft

Objective of present study is to analyse the coupled thermo-mechanical stresses in tapered FG shaft. Initially comparative study of FG shaft has carried out over steel shaft. Then, stress results are plotted for different values of power law index and speed and also time dependent stress are also presented.

5.5.1 Comparative study of tapered FG shaft over steel tapered shaft

It is essential to compare results of stainless steel and FG shaft to show effects of FG shaft over steel shaft. In this comparative study section temperature assumed is linear. Material properties are functions of temperature and radial direction only. Keeping all parameters (as in Table 5. 1) are same for both FG and steel analysis is done. Figure 5. 7 shows normal and shear stress in x and theta direction respectively for Stainless steel material. Normal stress is increasing along radius negatively, shear stress also increasing along radius positively. Figure 5. 8 and Figure 5. 9 shows normal and shear stress in x and theta direction respectively for FGM.

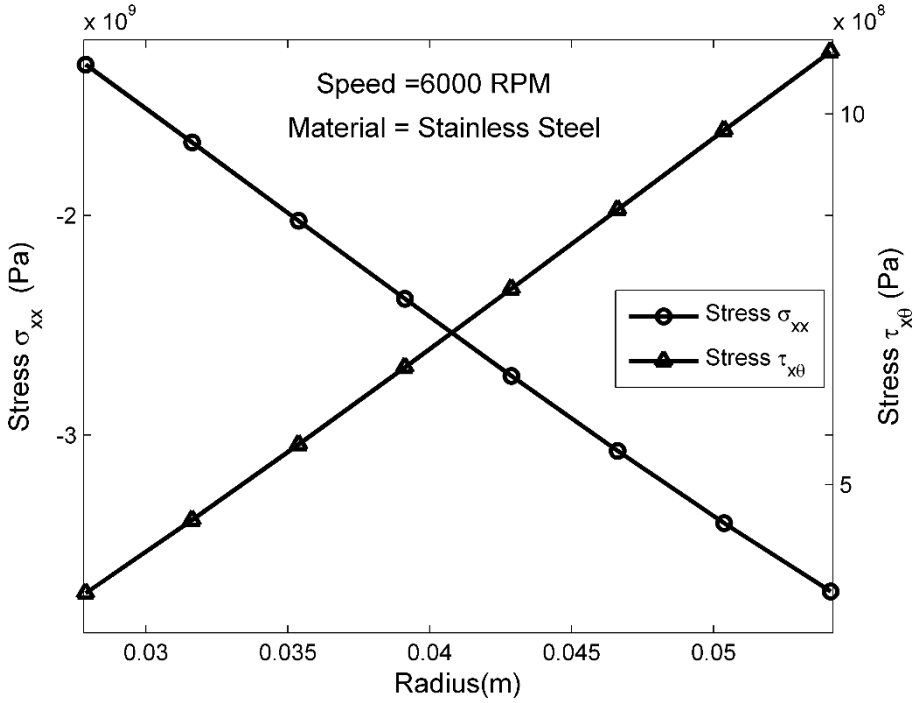

Figure 5. 7 Stress developed in tapered Steel shaft along radius.

Results are presented for shaft running at 6000 RPM, different 'k' values. It is easily seen from these Figures that, stress developed in FG shaft is lesser than Stainless steel shaft near outer surface of shaft. This conclusion influence to study FGMs.

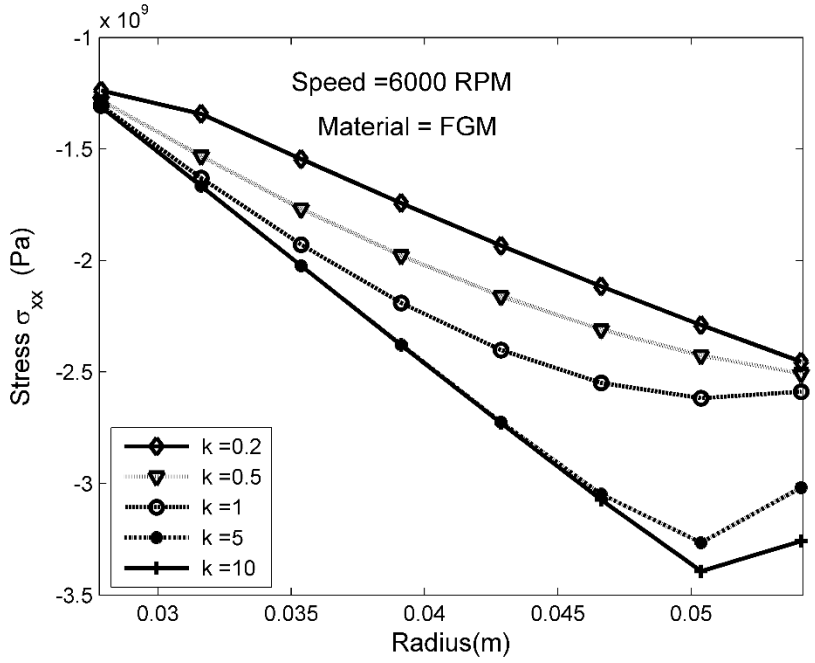

Figure 5. 8 Normal stress in tapered FG shaft along radius.

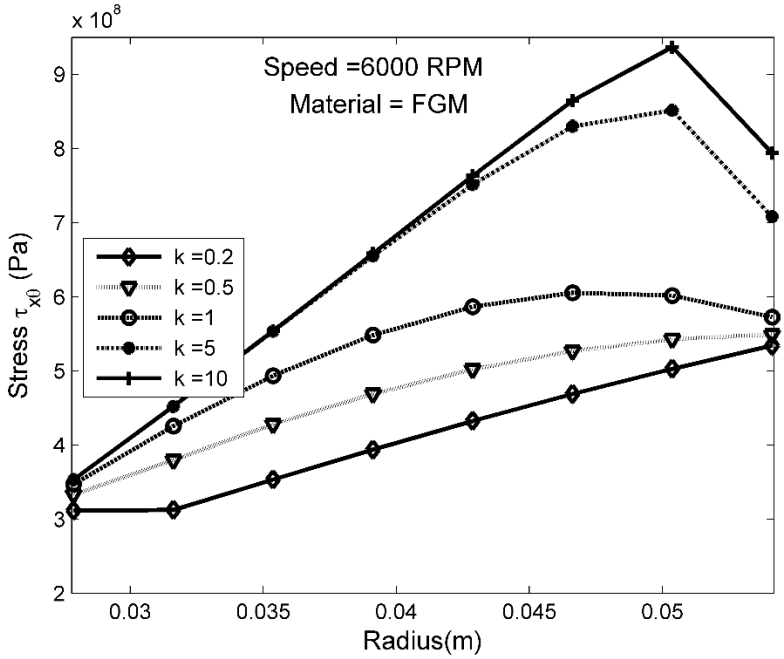

Figure 5. 9 Shear stress in tapered FG shaft along radius.

5.5.2 Variation of stresses for different values of 'k' in radial direction

In coupled thermal and mechanical environment, thermal strain is in coupled with only normal stress and shear stress in theta direction as in equation (21). Temperature dependent material properties are considered and temperature variation is as shown in Figure 5. 2. Figure 5. 10 (a) and (b) shows normal stress on plane perpendicular to x axis in x direction at 6000 RPM and 12000 RPM respectively. Maximum stress value is obtained at time t=0.008 sec and t=0.044 sec for 6000 RPM and 12000 Rpm respectively. Stress increases along radius of shaft negatively as thermal stress dominates mechanical stress in coupled environment. Also considering at a particular radius, normal stress is increases as 'k' value increases, because volume fraction of steel material is increases as power law index (k) increases. Fig (a) and Fig (b) are almost same but difference is, as speed increases amplitude in stress is more, which is shown and explained in succeeding section.

Figure 5. 10 (a) and (b) shows shear stress on plane perpendicular to x axis in theta direction at 6000 RPM and 12000 RPM respectively. Maximum stress values are obtained at time t=0.008 sec and t=0.044 sec for 6000 RPM and 12000 Rpm respectively. Shear stress increases along radius of shaft positively as thermal stress dominates mechanical stress in coupled environment. Also considering a particular radius, shear stress is increases as 'k' value increases, because volume fraction of steel material is increases as power law index (k) increases. Fig (a) and Fig (b) are

almost same but difference is, as speed increases fluctuation in stress is more, which is shown and explained in succeeding section.

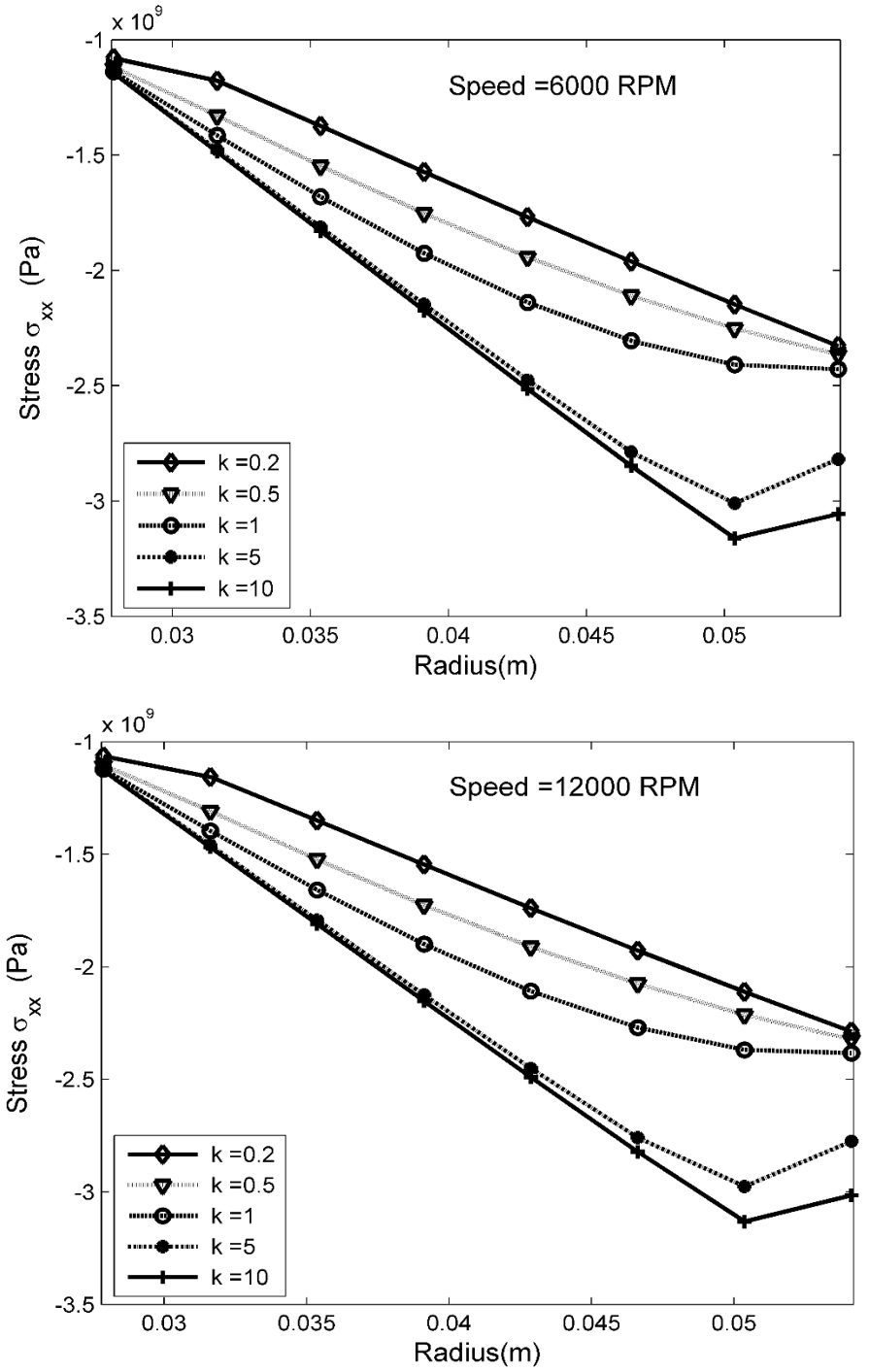

Figure 5. 10 Normal stress in tapered FG shaft along radius:
(a) At 6000 RPM, (b) At 12000 RPM

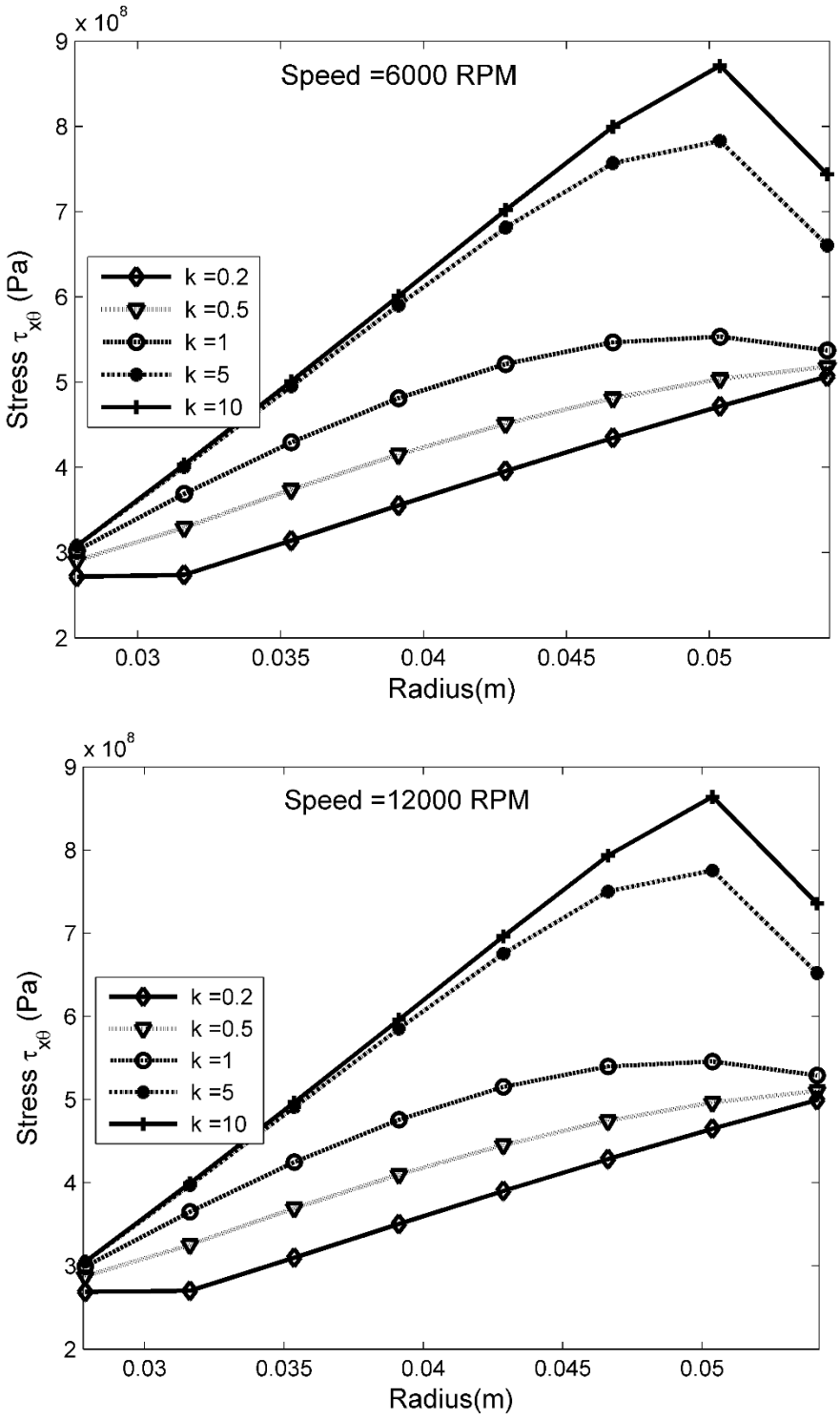

Figure 5. 11 Shear stress in tapered FG shaft along radius.
(a) At 6000 RPM, (b) at 12000 RPM

5.5.3 Transient uncoupled stress analysis for different value of power law index

Uncoupled (without considering thermal strain) transient stress obtained by equation (20) at the top of the surface. Considering temperature dependent material properties and temperature variation as in Figure 5. 2. Figure 5. 12 Shows normal stress on plane perpendicular to x axis in x direction, Figure 5. 13 and Figure 5. 14 shows shear stress on plane perpendicular to x axis in theta and radial direction respectively also (a) and (b) represents shaft running at 6000 RPM and 12000 RPM respectively. Maximum stress amplitude developed in tapered shaft for initial small time interval, then stress amplitude is decreases as time increases and maintain constant amplitude at speed 6000 RPM. For initial small time interval stress amplitude is smaller, as time increases stress amplitude increases then attains almost constant amplitude for shaft running at 12000 RPM. Also it can be seen that, as power law index increases stress amplitude increases, this is based on displacement. Also by looking at y axis values, stress amplitude increases as speed increases.

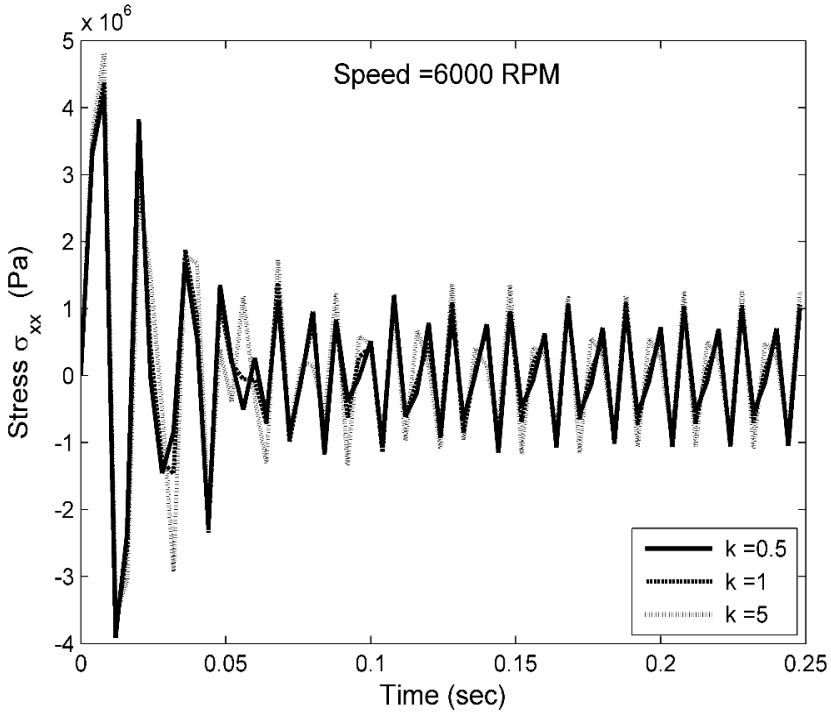

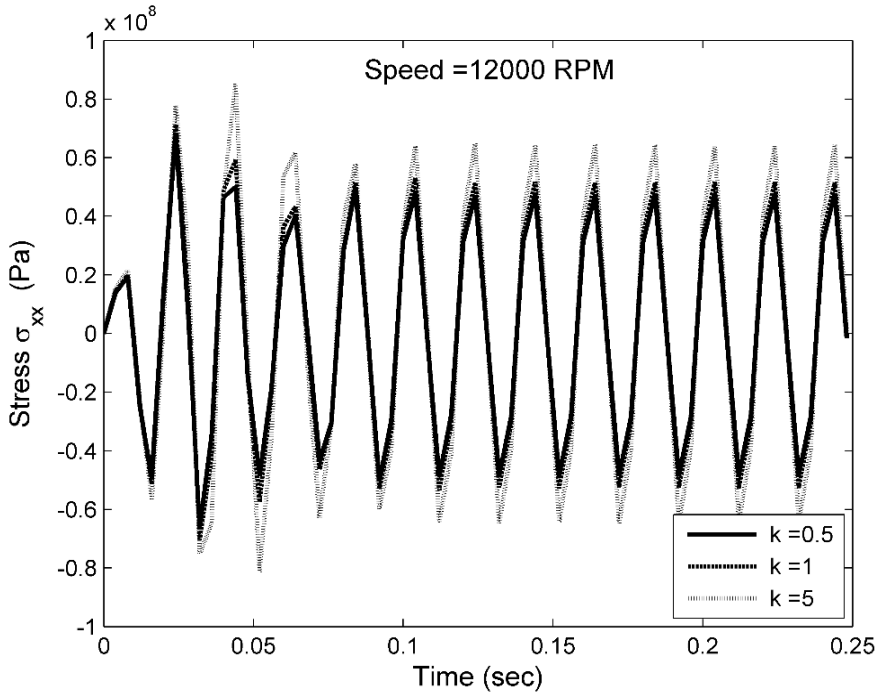

Figure 5. 12 Transient uncoupled normal stress in tapered FG shaft: (a) At 6000 RPM, (b) at 12000 RPM

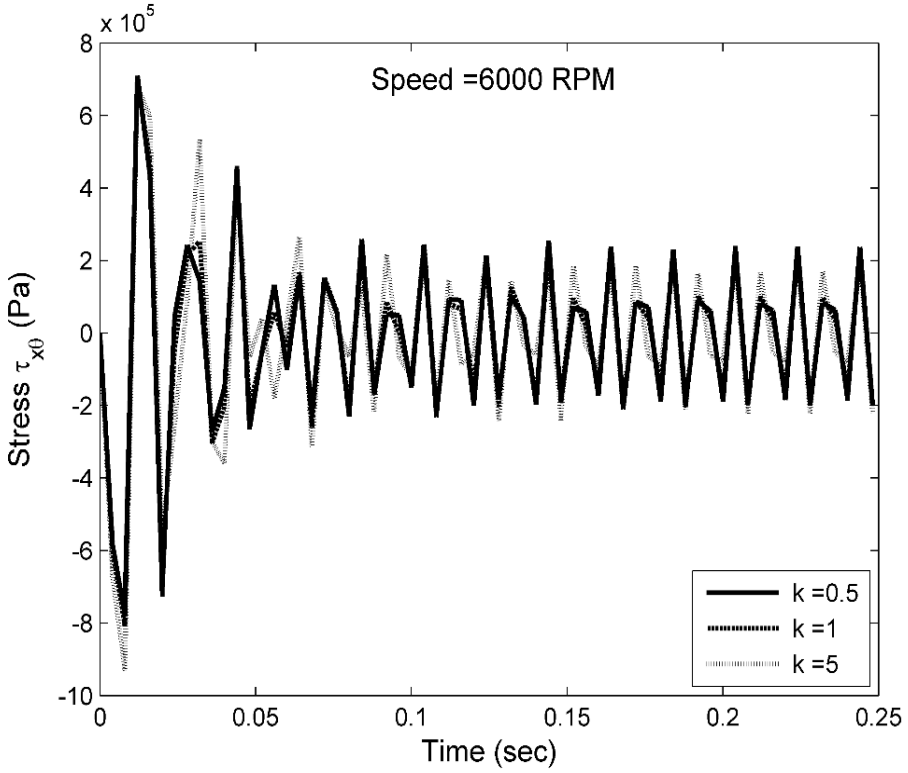

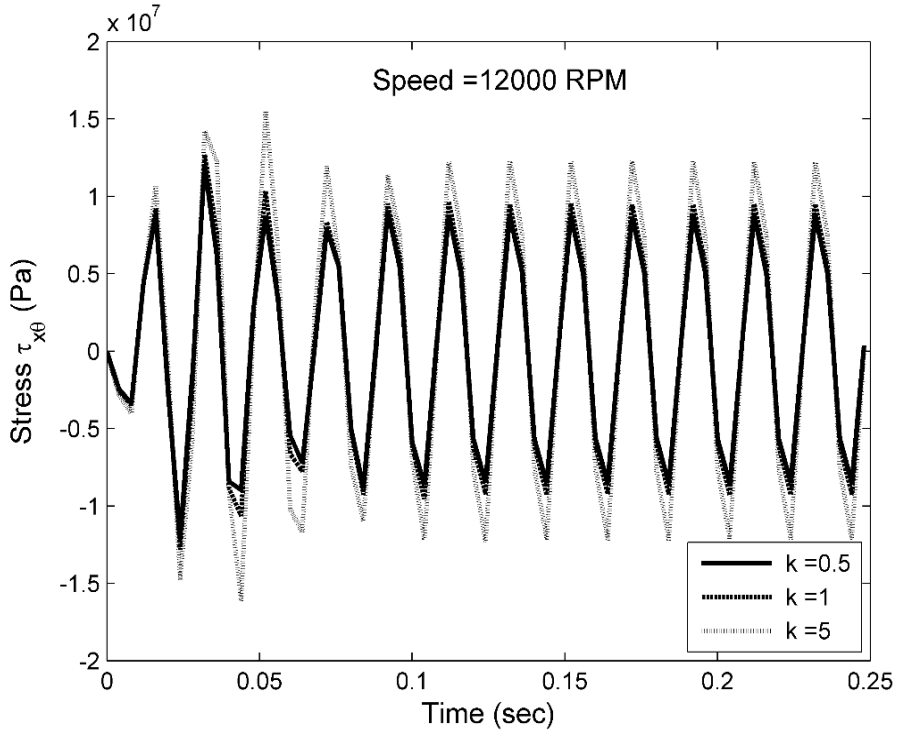

Figure 5. 13 Transient uncoupled shear stress in tapered FG shaft in theta direction: (a) At 6000 RPM, (b) at 12000 RPM

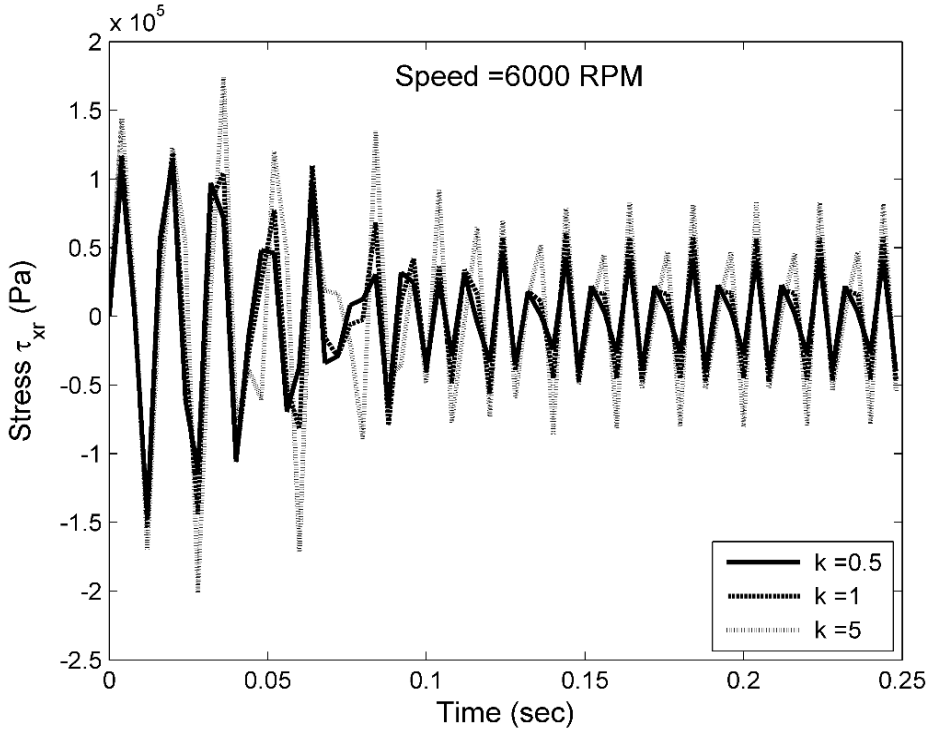

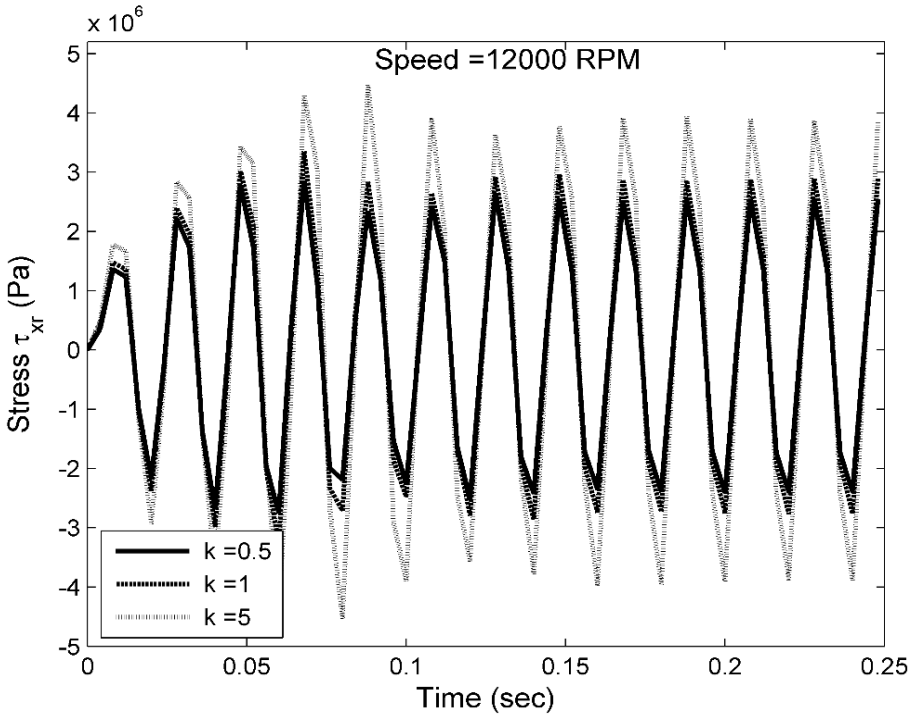

Figure 5. 14 Transient uncoupled shear stress in tapered FG shaft in radial direction: (a) At 6000 RPM, (b) at 12000 RPM

5.5.4 Transient coupled stress analysis for different value of power law index

Coupled (with considering thermal strain) transient stress obtained by equation (21) at the top of the surface. Considering temperature dependent material properties and temperature variation as in Figure 5. 2. Figure 5. 15 Shows normal stress on plane perpendicular to x axis in x direction, Figure 5. 16 shows shear stress on plane perpendicular to x axis in theta direction also (a) and (b) represents shaft running at 6000 RPM and 12000 RPM respectively. Maximum stress amplitude developed in tapered shaft for initial small time interval, then stress amplitude is decreases as time increases and maintain constant amplitude at speed 6000 RPM. For initial small time interval stress amplitude is smaller, as time increases stress amplitude increases then attains almost constant amplitude for shaft running at 12000 RPM. Also it can be seen that, as power law index increases stress amplitude increases, this is based on displacement. Also by looking at y axis values, stress amplitude increases as speed increases.

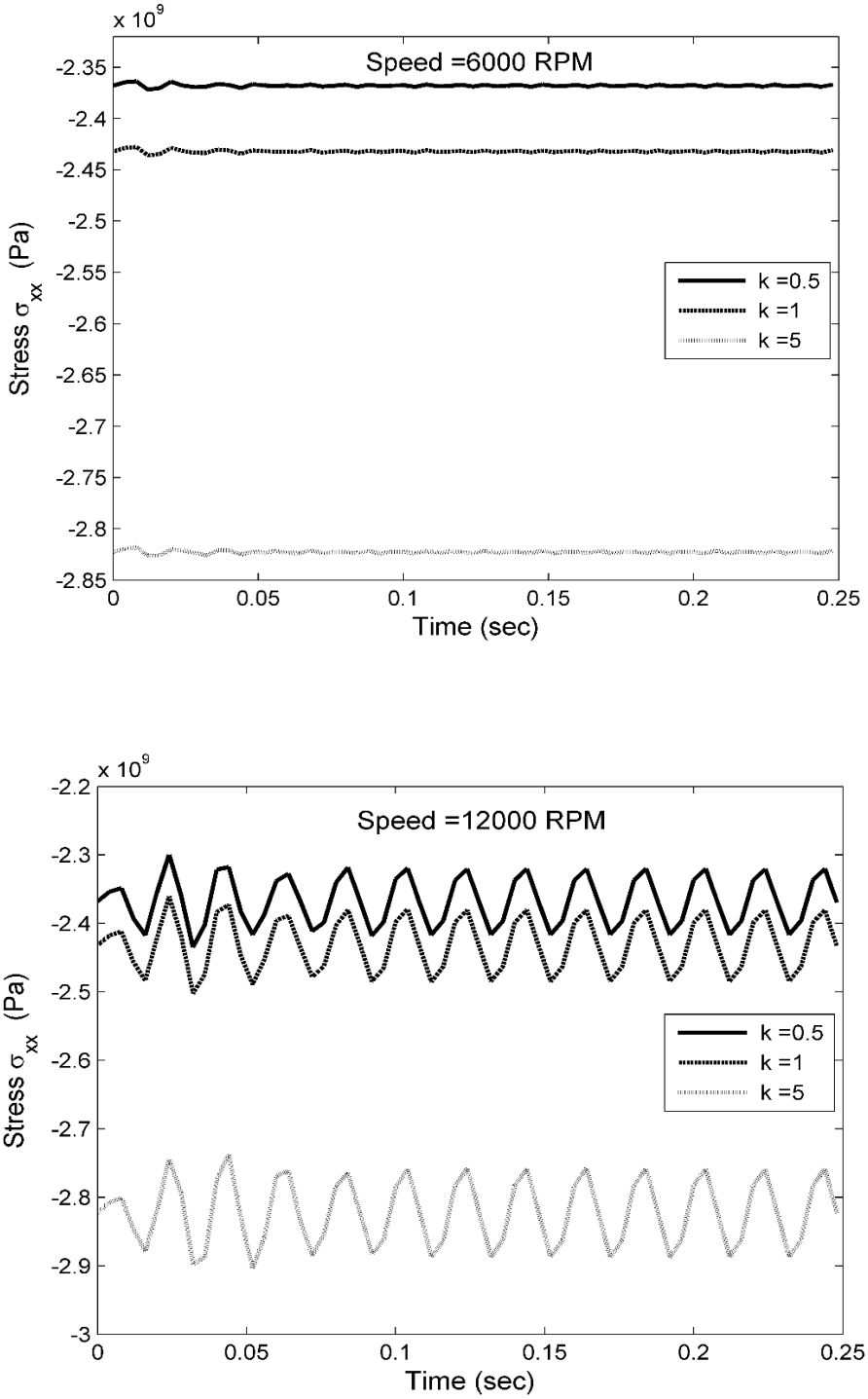

Figure 5. 15 Transient coupled normal stress in tapered FG shaft:
(a) At 6000 RPM, (b) At 12000 RPM

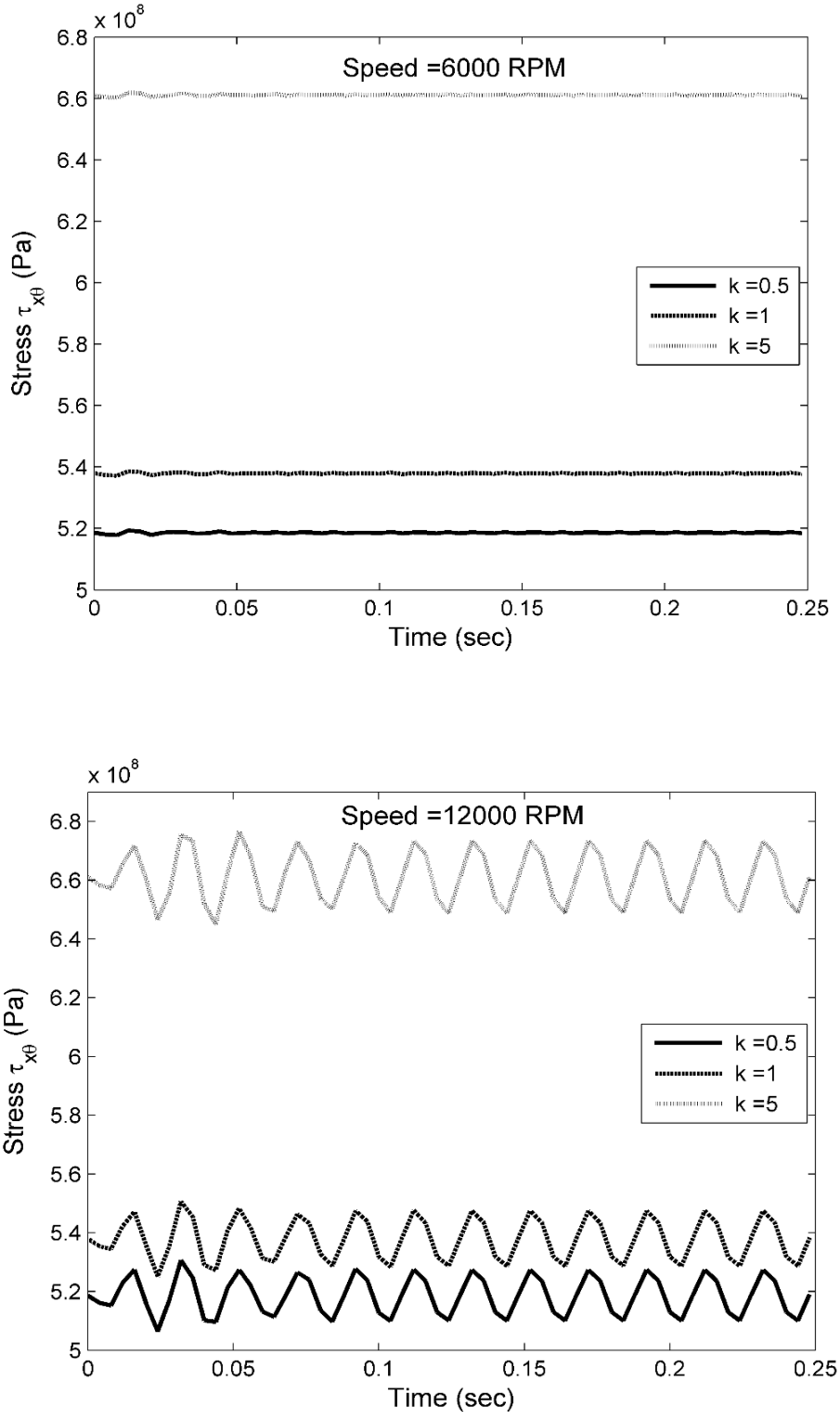

Figure 5. 16 Transient coupled shear stress in tapered FG shaft in theta direction: (a) At 6000 RPM, (b) At 12000 RPM

CHAPTER 6

CONCLUSION AND SCOPE OF FUTURE WORK

Important conclusions are drawn in this chapter based on above discussed results. Opportunity of future work is also been presented in this chapter.

6.1 Conclusions

Present study supports to draw following important conclusions.

i. Three nodded Timoshenko beam element has been implemented for modelling and analysis of FG tapered shaft by taking into account of structural damping and hysteretic damping in temperature environment.
ii. The temperature distribution is assumed based on one Dimensional steady state temperature field by using Fourier heat conduction equation without considering heat generation.
iii. Temperature dependent material properties are established by taking different power law index value.
iv. Stress values are compared between steel and FG shaft by taking temperature dependent material properties for linear variation of temperature, it is found that stresses developed in FG shaft is lower than Steel shaft.
v. It is also noted that stress increases as power law index increases.
vi. Stress amplitude increases as speed of the shaft increases.

6.2 Scope of future work

i. Nonlinear modelling of FG shaft.
ii. Active vibration control of FG shaft.
iii. Analysis and control of breathing crack in FG shaft.

Appendix

Now simplifying and arranging the above equation gives,

$$I_m(x)=\pi\sum_{i=1}^{n}\rho_i\,(r^2{}_{i+1}-r^2{}_i);\quad I_d(x)=\frac{\pi}{4}\sum_{i=1}^{n}\rho_i\,(r^4{}_{i+1}-r^4{}_i);\quad I_p(x)=\frac{\pi}{2}\sum_{i=1}^{n}\rho_i\,(r^4{}_{i+1}-r^4{}_i)$$

$$\delta u:\mathrm{I_m}\frac{\partial^2 u}{\partial t^2}-A_{11}\frac{\partial^2 u}{\partial x^2}-k_sB_{16}\frac{\partial^2\phi}{\partial x^2}+\sum_{i=1}^{N_D}I_{mi}^{D}\frac{\partial^2 v}{\partial t^2}\Delta(x-x_{Di})=R_x$$

$$\delta v:\mathrm{I_m}\frac{\partial^2 v}{\partial t^2}+k_s(A_{55}+A_{66})\left(\frac{\partial\beta_y}{\partial x}-\frac{\partial^2 v}{\partial x^2}\right)+\frac{1}{2}k_sB_{16}^2\frac{\partial^2\beta_x}{\partial x^2}+\sum_{i=1}^{N_D}I_{mi}^{D}\frac{\partial^2 v}{\partial t^2}\Delta(x-x_{Di})+P_v^b=R_y$$

$$\delta w:\mathrm{I_m}\frac{\partial^2 w}{\partial t^2}-k_s(A_{55}+A_{66})\left(\frac{\partial^2 w}{\partial x^2}+\frac{\partial\beta_x}{\partial x}\right)-\frac{1}{2}k_sB_{16}\frac{\partial^2\beta_y}{\partial x^2}+\sum_{i=1}^{N_D}I_{mi}^{D}\frac{\partial^2 w}{\partial t^2}\Delta(x-x_{Di})+P_w^b=R_z$$

$$\delta\beta_x:\begin{bmatrix}\mathrm{I}_d\frac{\partial^2\beta_x}{\partial t^2}+I_p\Omega\frac{\delta\beta_y}{\partial t}+\frac{1}{2}k_sB_{16}\frac{\partial^2 v}{\partial x^2}-D_{11}\frac{\partial^2\beta_x}{\partial x^2}+k_s(A_{55}+A_{66})\left(\frac{\partial w}{\partial x}+\beta_x\right)\\ -k_sB_{16}\frac{\partial\beta_y}{\partial x}+\sum_{i=1}^{N_D}\left(I_{di}^{D}\frac{\partial^2\beta_x}{\partial t^2}\right)\Delta(x-x_{Di})\end{bmatrix}=M_x$$

$$\delta\beta_y:\begin{bmatrix}\mathrm{I}_d\frac{\partial^2\beta_y}{\partial t^2}+I_p\Omega\frac{\delta\beta_x}{\partial t}+\frac{1}{2}k_sB_{16}^2\frac{\partial^2 w}{\partial x^2}-D_{11}\frac{\partial^2\beta_y}{\partial x^2}+k_s(A_{55}+A_{66})\left(\beta_y-\frac{\partial v}{\partial x}\right)\\ +k_sB_{16}\frac{\partial\beta_x}{\partial x}+\sum_{i=1}^{N_D}\left(I_{di}^{D}\frac{\partial^2\beta_y}{\partial t^2}\right)\Delta(x-x_{Di})\end{bmatrix}=M_y$$

$$\delta\phi:\mathrm{I}_p\frac{\partial^2\phi}{\partial t^2}-k_sB_{16}\frac{\partial^2 u}{\partial x^2}-k_sD_{66}\frac{\partial^2\phi}{\partial x^2}+\sum_{i=1}^{N_D}\left(I_{di}^{D}\frac{\partial^2\phi}{\partial t^2}\right)\Delta(x-x_{Di})=M_{x\theta}$$

Where

$$A_{11}(x)=\pi\sum_{i=1}^{n}C_{11i}\left(r_{i+1}^2-r_i^2\right);\quad A_{55}(x)=\frac{\pi}{2}\sum_{i=1}^{n}C_{55i}\left(r_{i+1}^2-r_i^2\right);\quad A_{66}(x)=\frac{\pi}{2}\sum_{i=1}^{n}C_{66i}\left(r_{i+1}^2-r_i^2\right)$$

$$B_{16}(x)=\frac{2\pi}{3}\sum_{i=1}^{n}C_{16i}\left(r_{i+1}^3-r_i^3\right);\quad D_{11}(x)=\frac{\pi}{4}\sum_{i=1}^{n}C_{11i}\left(r_{i+1}^4-r_i^4\right);\quad D_{66}(x)=\frac{\pi}{2}\sum_{i=1}^{n}C_{66i}\left(r_{i+1}^4-r_i^4\right)$$

Mass, stiffness, circulation and gyroscopic matrices of FG Timoshenko beam element.

The general displacement matrix $\left\{q^e\right\}$ is given by

$$\left\{q^e\right\}^T = \left\{\left\{U^e\right\}^T \left\{V^e\right\}^T \left\{W^e\right\}^T \left\{\beta_x^e\right\}^T \left\{\beta_y^e\right\}^T \left\{\phi^e\right\}^T\right\}_{1\times 18}$$

Elemental mass matrix

$$\left[M^e\right] = \begin{bmatrix} \left[M^{11}\right]_{3\times3} & [0]_{3\times3} & [0]_{3\times3} & [0]_{3\times3} & [0]_{3\times3} & [0]_{3\times3} \\ [0]_{3\times3} & \left[M^{22}\right]_{3\times3} & [0]_{3\times3} & [0]_{3\times3} & [0]_{3\times3} & [0]_{3\times3} \\ [0]_{3\times3} & [0]_{3\times3} & \left[M^{33}\right]_{3\times3} & [0]_{3\times3} & [0]_{3\times3} & [0]_{3\times3} \\ [0]_{3\times3} & [0]_{3\times3} & [0]_{3\times3} & \left[M^{44}\right]_{3\times3} & [0]_{3\times3} & [0]_{3\times3} \\ [0]_{3\times3} & [0]_{3\times3} & [0]_{3\times3} & [0]_{3\times3} & \left[M^{55}\right]_{3\times3} & [0]_{3\times3} \\ [0]_{3\times3} & [0]_{3\times3} & [0]_{3\times3} & [0]_{3\times3} & [0]_{3\times3} & \left[M^{66}\right]_{3\times3} \end{bmatrix}_{18\times18}$$

Where

$$M_{ij}^{11} = \int_{xa}^{xb} I_m \psi_i \psi_j dx = M_{ij}^{22} = M_{ij}^{33}; M_{ij}^{44} = \int_{xa}^{xb} I_d \psi_i \psi_j dx = M_{ij}^{55}; \quad M_{ij}^{66} = \int_{xa}^{xb} I_p \psi_i \psi_j dx$$

Elemental stiffness matrix

$$\left[K^e\right] = \begin{bmatrix} \left[K^{11}\right]_{3\times3} & [0]_{3\times3} & [0]_{3\times3} & [0]_{3\times3} & [0]_{3\times3} & \left[K^{16}\right]_{3\times3} \\ [0]_{3\times3} & \left[K^{22}\right]_{3\times3} & [0]_{3\times3} & \left[K^{24}\right]_{3\times3} & \left[K^{25}\right]_{3\times3} & [0]_{3\times3} \\ [0]_{3\times3} & [0]_{3\times3} & \left[K^{33}\right]_{3\times3} & \left[K^{34}\right]_{3\times3} & \left[K^{35}\right]_{3\times3} & [0]_{3\times3} \\ [0]_{3\times3} & \left[K^{42}\right]_{3\times3} & \left[K^{43}\right]_{3\times3} & \left[K^{44}\right]_{3\times3} & \left[K^{45}\right]_{3\times3} & [0]_{3\times3} \\ [0]_{3\times3} & \left[K^{52}\right]_{3\times3} & \left[K^{53}\right]_{3\times3} & \left[K^{54}\right]_{3\times3} & \left[K^{55}\right]_{3\times3} & [0]_{3\times3} \\ \left[K^{61}\right]_{3\times3} & [0]_{3\times3} & [0]_{3\times3} & [0]_{3\times3} & [0]_{3\times3} & \left[K^{66}\right]_{3\times3} \end{bmatrix}_{18\times18}$$

Where

$$K_{ij}^{11} = \int_{xa}^{xb} A_{11} \frac{\partial \psi_i}{\partial x} \frac{\partial \psi_j}{\partial x} dx; \quad K_{ij}^{16} = \int_{xa}^{xb} k_s B_{16} \frac{\partial \psi_i}{\partial x} \frac{\partial \psi_j}{\partial x} dx$$

$$K_{ij}^{22} = \int_{xa}^{xb} k_s \left(A_{55} + A_{66}\right) \frac{\partial \psi_i}{\partial x} \frac{\partial \psi_j}{\partial x} dx; \quad K_{ij}^{24} = \int_{xa}^{xb} -\frac{1}{2} k_s B_{16} \frac{\partial \psi_i}{\partial x} \frac{\partial \psi_j}{\partial x} dx$$

$$K_{ij}^{25}=\int_{xa}^{xb}-k_s\left(A_{55}+A_{66}\right)\frac{\partial\psi_i}{\partial x}\psi_j dx$$

$$K_{ij}^{33}=\int_{xa}^{xb}k_s\left(A_{55}+A_{66}\right)\frac{\partial\psi_i}{\partial x}\frac{\partial\psi_j}{\partial x}dx;\quad K_{ij}^{34}=\int_{xa}^{xb}k_s\left(A_{55}+A_{66}\right)\frac{\partial\psi_i}{\partial x}\psi_j dx\ K_{ij}^{35}=\int_{xa}^{xb}-\frac{1}{2}k_sB_{16}\frac{\partial\psi_i}{\partial x}\frac{\partial\psi_j}{\partial x}dx$$

$$;\ K_{ij}^{42}=\int_{xa}^{xb}-\frac{1}{2}k_sB_{16}\frac{\partial\psi_i}{\partial x}\frac{\partial\psi_j}{\partial x}dx;\quad K_{ij}^{43}=\int_{xa}^{xb}k_s\left(A_{55}+A_{66}\right)\psi_i\frac{\partial\psi_j}{\partial x}dx$$

$$K_{ij}^{44}=\int_{xa}^{xb}\left\{k_s\left(A_{55}+A_{66}\right)\psi_i\psi_j+D_{11}\frac{\partial\psi_i}{\partial x}\frac{\partial\psi_j}{\partial x}\right\}dx;\quad K_{ij}^{45}=\int_{xa}^{xb}\left\{\frac{1}{2}k_sB_{16}\frac{\partial\psi_i}{\partial x}\psi_j-\frac{1}{2}k_sB_{16}\psi_i\frac{\partial\psi_j}{\partial x}\right\}dx$$

$$K_{ij}^{52}=\int_{xa}^{xb}-k_s\left(A_{55}+A_{66}\right)\psi_i\frac{\partial\psi_j}{\partial x}dx;\quad K_{ij}^{53}=\int_{xa}^{xb}-\frac{1}{2}k_sB_{16}\frac{\partial\psi_i}{\partial x}\frac{\partial\psi_j}{\partial x}dx$$

$$K_{ij}^{54}=\int_{xa}^{xb}\left\{-\frac{1}{2}k_sB_{16}\frac{\partial\psi_i}{\partial x}\psi_j+\frac{1}{2}k_sB_{16}\psi_i\frac{\partial\psi_j}{\partial x}\right\}dx;\quad K_{ij}^{55}=\int_{xa}^{xb}\left\{k_s\left(A_{55}+A_{66}\right)\psi_i\psi_j+D_{11}\frac{\partial\psi_i}{\partial x}\frac{\partial\psi_j}{\partial x}\right\}dx$$

$$K_{ij}^{61}=\int_{xa}^{xb}k_sB_{16}\frac{\partial\psi_i}{\partial x}\frac{\partial\psi_j}{\partial x}dx;\quad K_{ij}^{66}=\int_{xa}^{xb}k_sD_{66}\frac{\partial\psi_i}{\partial x}\frac{\partial\psi_j}{\partial x}dx$$

Circulatory stiffness matrix

$$\left[K_{cir}\right]_{18\times18}=\int_{x_i}^{x_j}M^T\xi M dx$$

Where

$$\left[M\right]=\begin{bmatrix}\psi_1&\psi_2&\psi_3&0&0&0&0&0&0&0&0&0&0&0&0&0&0&0\\0&0&0&\psi_1'&\psi_2'&\psi_3'&0&0&0&0&0&0&\psi_1'&\psi_2'&\psi_3'&0&0&0\\0&0&0&0&0&0&\psi_1'&\psi_2'&\psi_3'&-\psi_1'&-\psi_2'&-\psi_3'&0&0&0&0&0&0\\0&0&0&0&0&0&\psi_1''&\psi_2''&\psi_3''&-\psi_1''&-\psi_2''&-\psi_3''&0&0&0&0&0&0\\0&0&0&\psi_1''&\psi_2''&\psi_3''&0&0&0&0&0&0&\psi_1''&\psi_2''&\psi_3''&0&0&0\\0&0&0&0&0&0&0&0&0&0&0&0&0&0&0&\psi_1&\psi_2&\psi_3\end{bmatrix}_{6\times18}$$

$$\left[\xi\right]=\begin{bmatrix}0&0&0&0&0&0\\0&0&GA&0&0&0\\0&-GA&0&0&0&0\\0&0&0&0&EI&0\\0&0&0&-EI&0&0\\0&0&0&0&0&0\end{bmatrix}_{6\times6}$$

Gyroscopic matrix

$$\left[G^e\right]=\begin{bmatrix}
\left[0\right]_{3\times3} & \left[0\right]_{3\times3} & \left[0\right]_{3\times3} & \left[0\right]_{3\times3} & \left[0\right]_{3\times3} & \left[0\right]_{3\times3}\\
\left[0\right]_{3\times3} & \left[0\right]_{3\times3} & \left[0\right]_{3\times3} & \left[0\right]_{3\times3} & \left[0\right]_{3\times3} & \left[0\right]_{3\times3}\\
\left[0\right]_{3\times3} & \left[0\right]_{3\times3} & \left[0\right]_{3\times3} & \left[0\right]_{3\times3} & \left[0\right]_{3\times3} & \left[0\right]_{3\times3}\\
\left[0\right]_{3\times3} & \left[0\right]_{3\times3} & \left[0\right]_{3\times3} & \left[0\right]_{3\times3} & \left[G^{45}\right]_{3\times3} & \left[0\right]_{3\times3}\\
\left[0\right]_{3\times3} & \left[0\right]_{3\times3} & \left[0\right]_{3\times3} & \left[G^{54}\right]_{3\times3} & \left[0\right]_{3\times3} & \left[0\right]_{3\times3}\\
\left[0\right]_{3\times3} & \left[0\right]_{3\times3} & \left[0\right]_{3\times3} & \left[0\right]_{3\times3} & \left[0\right]_{3\times3} & \left[0\right]_{3\times3}
\end{bmatrix}_{18\times18}$$

$$G_{ij}^{45}=\int_{xa}^{xb} I_p\psi_i\psi_j dx;\qquad G_{ij}^{54}=\int_{xa}^{xb} -I_p\psi_i\psi_j dx$$

References

1. Y.Miyamoto, W.A.Kaysser, B.H.Rabin, A.Kawasaki and R.G.Ford, Functionally Graded Materials: Design, Processing and Applications, *Kluwer Academic Publishers*, London, **1999**.
2. Schmauder S. and Weber U. Modelling of functionally graded materials by numerical homogenization, Archive of Applied Mechanics, 71(**2001**): pp. 182-192.
3. Sladek J., Sladek V. and Zhang Ch. Transient Heat Conduction Analysis in Functionally Graded Materials by the Meshless Local Boundary Integral Equation Method, *Computational Materials Science*, 28(**2003**): pp.494-504.
4. Shao Z.S. and Ma G.W. Thermo-mechanical Stresses in Functionally Graded Circular Hollow Cylinder with Linearly Increasing Boundary Temperature, *Composite Structures*, 83(**2008**): pp. 259-265.
5. Farhatnia Fatemesh, Sharifi Gholam-Ali and Rasouli Saeid. Numerical and Analytical Approach of Theromechanical Stresses in FGM Beams, *Proceedings of the World Congress on Engineering*, 2(**2009**): pp. 1-6.
6. Jyothula Suresh., Bathini Sidda., Bathini Eshwara Reddy C. and Kontakkagari VIjaya Kumar. Nonlinear Thermal Analysis of Functionally Graded Plated Using Higher Order Theory, *Innovative Systems Design and Engineering*, 2(**2011**): pp. 1-14.
7. Callioglu Hasan. Stress Analysis in a Functionally Graded Disc under Mechanical Loads and a Steady State Temperature Distribution, *Sadhana*, 36(**2011**): pp. 53-64.
8. Abotula Sandeep, Kidane Addis, Chalivendra Vijaya B. and Shukla Arun, Dynamic Curving Cracks in Functionally Graded Materials Under Thermo-Mechanical Loading, *International Journal of Solids and Structures*, 49(**2012**): pp. 1637-1655.
9. Bhandari Manish and Dr. Purohit Kamlesh, Analysis of Functionally Graded Material Plate Under Transverse Load for Various Boundary Conditions, *Journal of Mechanical and Civil Engineering*, 10(**2014**): pp. 46-55.
10. Kursun A., Kara E., Cetin E., Aksoy S. and Kesimli A. Mechanical and Thermal Stresses in Functionally Graded Cylinders, *International Journal of Mechanical, Aerospace, Industrial and Mechatronics Engineering*, 8(**2014**): pp. 301-306.

11. Woo J. and Meguid S.A. Nonlinear Analysis of Functionally Graded Plates and Shallow Shells, *International Journal of Solids and Structures*, 28(**2001**): pp. 7409-7421.
12. Reddy J.N. and Cheng Zhen-Qiang, Three-dimensional Thermomechanical Deformations of Functionally Graded Rectangular Plates, *Eur. J. Mech. A/Solids* 20(**2001**): pp. 841-855.
13. Jin Z. H. and Paulino Glaucio H. Transient Thermal Stress Analysis of an Edge Crack in a Functionally Graded Material, *International Journal of Fracture*, 107(**2001**): pp. 73-98.
14. Chakraborty A., Gopalakrishnan S. and Reddy J.N. A New Beam Finite Element for the Analysis of Functionally Graded Materials, *International Journal of Mechanical sciences*, 45(**2003**): pp. 519-539.
15. Vel Senthil S. and Batra R.C. Three-dimensional Analysis of Transient Thermal Stresses in Functionally Graded Plates, *International Journal of Solids and Structures*, 40(**2003**): pp. 7181-7196.
16. Wang Hui and Qin Qing-Hua. Meshless Approach for Thermo-Mechanical Analysis of Functionally Graded Materials, *Engineering Analysis with Boundary Elements*, 32(**2008**): pp. 704-712.
17. Tahani Masoud, Mahmoud Seyed, Safari Ali and Todoroki Akira. Transient and Dynamic Stress Analysis Of Functionally Graded Thick Hollow Cylinder Subjected To Thermal Shock Loading Using An Analytical Method, *Journal of Solid Mechanics Engineering*, 4(**2008**): pp. 1346-1359.
18. Gupta Sachin, Abotula Sandeep, Chalivendra Vijaya B., Shukla Arun and Chona Ravi. Transient Thermo-mechanical Analysis of Dynamic Curving Cracks in Functionally Graded Materials, *Acta Mech*, 23(**2012**): pp. 1485-1506.
19. Zorzi E.S. and Nelson H.D. Finite Element Simulation of Rotor Bearing Systems with Internal Damping, *Journal of Engineering for Gas Turbines and Power*, 99(**1976**): pp.71-76.
20. Zorzi E. S. and Nelson H.D. Finite Element Simulation of Rotor Bearing Systems with Internal Damping, *American Society of Mechanical Engineers*, (**1977**): pp. 71-76.
21. Rouch K. E. and Kao J. S. A Tapered Beam Finite Element for Rotor Dynamics Analysis, *Journal of sound and vibration*, 66(**1979**): pp. 119-140.
22. Kim Chun-Do and Bert Charles W. Critical Speed Analysis of Laminated Composite, Hollow Drive Shafts. *Composites engineering*, 3(**1993**): pp. 633-643.

23. Bert Charles W. and Kim Chun-Do. Analysis of Buckling of Hollow Laminated Composite Drive Shaft. *Composite science and technology*, 53(**1995**): pp. 343-351.
24. Dimarogonas Andrew D. Vibration of Cracked Structures: A State of the Art Review, *Engineering Fracture Mechanics*, 55(**1996**): pp. 831-857.
25. Singh S. P. and Gupta K. Composite Shaft Rotor Dynamic Analysis Using Layer Wise Theory, *Journal of sound and vibration*, 191(**1996**): 739-756.
26. Wettergren H. L. and Olsson K. O. Viscous Damping Supported in Anisotropic Bearing, *Journal of sound and vibration*, 195(**1996**): 75-84.
27. Abduljabbar Z., Eimadany M. M. and Al-Bahkali E. On the Vibration And Control of a Flexible Rotor Mounted On Fluid Film Bearings, *Computers and Structures*, 65(**1997**): pp. 849-856.
28. Reddy J.N. and Chin C.D. Thermomechanical Analysis of Functionally Graded Cylinders and Plates, *Journal of Thermal Stresses*, 21(**1998**): pp. 593-626.
29. Liew K. M., Kitipornchai S., Zhang X. Z. and Lim C. W. Analysis of the Thermal Stress Behaviour of Functionally Graded Hollow Circular Cylinders, *International Journal of Solids and Structures*, 40(**2003**): pp. 2355-2380.
30. Lin Chi-Wei, Tu Jay F. and Kamman Joe. An Integrated Thermo-Mechanical-Dynamic Model to Characterize Motorized Machine Tool Spindles During Very High Speed Rotation, *International Journal of machine tools & manufacture*, 43(**2003**): pp. 1035-1050.
31. Chang Min-Yung, Chen Jeng-Keag and Chang Chih-Yung. A Simple Spinning Laminated Composite Shaft Model, *International Journal of Solids and Structures*, 41(**2004**): pp. 637-662.
32. Shokrieh Mahmood M., Hasani Akbar and Lessard Larry B. Shear Buckling of a Composite Drive Shaft Under Torsion, *Composite Structures*, 64(**2004**): pp. 63-69.
33. Shao Z. S. Mechanical and Thermal Stresses of Functionally Graded Circular Hollow Cylinder with Finite Length, *International journal of pressure vessels and piping*, 82(**2005**): pp. 155-163.
34. Shao Z. S. and Ma G. W. Thermo-mechanical Stresses in Functionally Graded Circular Hollow Cylinder with Linearly Increasing Boundary Temperature, *Composite Structures*, 83(**2008**): pp. 259-265.

35. Das A. S., Nighil M. C., Dutt J. K. and Irretier H. Vibration Control and Stability Analysis of Rotor-Shaft System with Electromagnetic Exciters, *Mechanisms and Machine Theory*, 43(**2008**): pp. 1295-1316.
36. Xiang H. J. and Yang J. Free and Forced Vibration of a Laminated FGM Timoshenko Beam of Variable Thickness under Heat Conduction, *Composites Structures*, 39(**2008**): pp. 292-303.
37. Roy H., Dutt J. K. and Datta P. K. Dynamics of a Viscoelastic Rotor Shaft Augmenting Thermodynamic Fields – A Finite Element Approach. *International Journal of Mechanical Sciences*. 50(**2008**): pp. 845-853.
38. Bayat Mehdi, Sahari B. B., Saleem M., Hamouda A. M. S. and Reddy J. N. Thermo Elastic Analysis of Functionally Graded Rotating Disks with Temperature-Dependent Material Properties: Uniform And Variable Thickness, *Int J Mech Mater Des*, 5(**2009**): pp. 263-279.
39. Badie M. A., Mahdi E., Hamouda A. M. S. An Investigation into Hybrid Carbon/Glass Fibre Reinforced Epoxy Composite Automotive Drive Shaft. *Materials and Design*, 32(**2011**): pp. 1485-1500.
40. Poursaeidi Esmaeil and Yazdi Mostafa Kamalzadeh. Causes of Rotor Distortions and Applicable Common Straightening Methods for Turbine Rotors and Shafts, *World Academy of science, Engineering and Technology*, 5(**2011**): pp. 156-161.
41. Sheihlou Mehrdad, Rezazadeh Ghader and Shabani Rasool. Study of Torsional Vibrational Vibration of a Radially FGM Micro-Shaft, *International journal of mechanic systems engineering*, 3(**2013**): pp. 1-5.
42. Rao D. Koteswara, Roy Tarapada, Gayen Debabrata and Inamdar Prasad K. Finite Element Analysis of Functionally Graded Rotor Shaft Using Timoshenko Beam Theory. International *Journal of Mechanical and production Engineering*. 1(**2013**): pp. 10-14.
43. Prakash T., Singha M. K. and Ganapathi M., Thermal Postbuckling Analysis of FGM Skew Plates. *Engineering and Structures*. 1(**2008**): pp. 22-32.
44. Alshorbagy Amal E., Eltaher M.A. and Mahmoud F.F. Free Vibration Characteristics of a Functionally Graded Beam by Finite Element Method, *Applied Mathematical Modelling*, 35(**2011**): pp. 412-425.